

On the AGB stars of M 4: A robust disagreement between spectroscopic observations and theory

B. T. MacLean^{1*}, S. W. Campbell¹, A. M. Amarsi², T. Nordlander^{3,4},
P. L. Cottrell^{1,5}, G. M. De Silva^{6,7}, J. Lattanzio¹, T. Constantino^{8,1},
V. D’Orazi^{9,10,11} and L. Casagrande^{3,4}

¹Monash Centre for Astrophysics, School of Physics and Astronomy, Monash University, Victoria 3800, Australia

²Max Planck Institute für Astronomy, Königstuhl 17, D-69117 Heidelberg, Germany

³Research School of Astronomy and Astrophysics, Australian National University, Canberra, ACT 2611, Australia

⁴ARC Centre of Excellence for All Sky Astrophysics in 3 Dimensions (ASTRO 3D)

⁵School of Physical and Chemical Sciences, University of Canterbury, Private Bag 4800, Christchurch 8140, New Zealand

⁶Australian Astronomical Observatory, 105 Delhi Rd, North Ryde, NSW 2113, Australia

⁷Sydney Institute for Astronomy, School of Physics, The University of Sydney, NSW 2006, Australia

⁸Physics and Astronomy, University of Exeter, Exeter, EX4 4QL, United Kingdom

⁹INAF Osservatorio Astronomico di Padova, vicolo dell’Osservatorio 5, I-35122, Padova, Italy

¹⁰Research Centre for Astronomy, Astrophysics & Astrophotonics (MQAAAstro), Macquarie University, Sydney, NSW 2109, Australia

¹¹Department of Physics and Astronomy, Macquarie University, North Ryde, NSW 2109, Australia

Accepted TBC. Received TBC; in original form TBC

ABSTRACT

Several recent spectroscopic investigations have presented conflicting results on the existence of Na-rich asymptotic giant branch (AGB) stars in the Galactic globular cluster M 4 (NGC 6121). The studies disagree on whether or not Na-rich red giant branch (RGB) stars evolve to the AGB. For a sample of previously published HERMES/AAT AGB and RGB stellar spectra we present a re-analysis of O, Na, and Fe abundances, and a new analysis of Mg and Al abundances; we also present CN band strengths for this sample, derived from low-resolution AAOmega spectra. Following a detailed literature comparison, we find that the AGB samples of all studies consistently show lower abundances of Na and Al, and are weaker in CN, than RGB stars in the cluster. This is similar to recent observations of AGB stars in NGC 6752 and M 62. In an attempt to explain this result, we present new theoretical stellar evolutionary models for M 4; however, these predict that all stars, including Na-rich RGB stars, evolve onto the AGB. We test the robustness of our abundance results using a variety of atmospheric models and spectroscopic methods; however, we do not find evidence that systematic modelling uncertainties can explain the apparent lack of Na-rich AGB stars in M 4. We conclude that an unexplained, but robust, discordance between observations and theory remains for the AGB stars in M 4.

Key words: Galaxy: formation – Galaxy: abundances – Galaxy: globular clusters: general – stars: abundances – stars: AGB and post-AGB.

1 INTRODUCTION

In early GC studies stars were observed at the same evolutionary stage but with different CN strengths, which cannot be explained only with evolutionary effects (e.g. Hesser et al. 1977; Norris et al. 1981). These and other findings led to the general consensus that Galactic GCs contain multiple populations of stars, identified by variations in light elemental

abundances that are *intrinsic* – inherited at birth – to the stars. Variations are typically observed in the abundances of C, N, Na, and O, and sometimes Mg and Al (see the extensive reviews of Sneden 1999; Gratton et al. 2012 and references therein; but see Bastian et al. 2013 for an opposing view). In this paper we designate those GC stars with halo-like abundances (CN-weak, Na poor) as subpopulation one (SP1), and all stars enriched in Na (or that present as CN-strong) as subpopulation two (SP2).

Over the decades since the first spectroscopic stud-

* E-mail: ben.maclean@monash.edu

ies of Galactic GCs, stars in each evolutionary phase have been targeted to evaluate the consistency of the light-elemental abundance distributions along the stellar evolutionary tracks. While systematic observations of the asymptotic giant branch (AGB, the final phase of nuclear burning) have only been performed relatively recently, AGB stars had previously been included among the GC stellar samples of last century. The literature reviews of [Snedden et al. \(2000\)](#) and [Campbell et al. \(2006\)](#) noted that the distribution of CN band strengths of AGB stars in certain globular clusters are very different to those seen in RGB stars – most strikingly that the AGB stars of NGC 6752 are exclusively CN-weak. This is in contradiction to the theoretical prediction that the N abundance of a star, which is traced by the CN band strength, should *increase* as a result of ‘deep mixing’ on the RGB ([Langer et al. 1985](#); [Henkel et al. 2017](#)).

Seeking a more reliable diagnostic tool, [Campbell et al. \(2013\)](#) measured Na abundances for a sample of 20 AGB and 24 RGB stars in NGC 6752. Just as in the earlier low-resolution CN studies of the cluster, they found homogeneity in their entire sample of AGB stars: the $[\text{Na}/\text{Fe}]$ values were all within ± 0.1 dex and very low ($[\text{Na}/\text{Fe}] \lesssim 0.12$ dex). This contrasted greatly with their RGB sample for which a variation in $[\text{Na}/\text{Fe}]$ of ~ 0.9 dex was reported. While this result was challenged observationally ([Lapenna et al. 2016](#)), a detailed reanalysis by [Campbell et al. \(2017, hereafter C17\)](#) supported the original conclusion: that up to 100% of the Na enhanced stars (SP2; which represent 70% of the total RGB population) in NGC 6752 appear to be avoiding the AGB entirely.

It is generally agreed that stars enriched in N and Na are also enriched in He ([Dupree et al. 2011](#); [Nardiello et al. 2015](#)). Stars with a He-enhancement evolve faster and thus have lower initial masses than stars of the same age but normal helium. Assuming these stars experience the same amount of mass loss on the RGB, they will retain less envelope on the horizontal branch (HB) and appear bluer ([Sweigart 1997](#); [Catelan 2009](#)).

The results of [Campbell et al. \(2013\)](#) conflict with the prediction of stellar evolutionary theory that only HB stars with extremely thin envelopes avoid the AGB, becoming AGB-manqué stars ([Renzini & Buzzoni 1986](#); [Greggio & Renzini 1990](#)). At the metallicities of GCs this only occurs in stellar models with effective temperatures (T_{eff}) higher than $\sim 15,000$ K ([Dorman et al. 1993](#)), corresponding to $\sim 30\%$ of the most helium enhanced stars in NGC 6752. Efforts to explain these observations have not been able to reproduce the results – see for example [Cassisi et al. \(2014\)](#), who could not reproduce the NGC 6752 observations using population synthesis (also see [Campbell et al. 2013](#); [Chantereau et al. 2016](#)).

Adding to the debate on this topic, [MacLean et al. \(2016, hereafter ML16\)](#) reported O, Na, and Fe abundances for a sample of 15 AGB and 106 RGB stars in M 4 (NGC 6121), which contains no HB stars predicted to become AGB-manqué stars – M 4’s HB extends only to ~ 9000 K in T_{eff} . Surprisingly, all 15 AGB stars were found to have SP1-like O and Na abundances despite a significantly larger spread in the RGB abundances. This is the third such finding (after NGC 6752 and M 62) of a paucity of SP2 AGB stars in a globular cluster; but the first for a GC without an extended blue HB. While AGB stars have been

included within stellar samples of spectroscopic M 4 studies in the past ([Norris 1981](#); [Suntzeff & Smith 1991](#); [Ivans et al. 1999](#); and the literature reviews of [Snedden et al. 2000](#); [Smith & Briley 2005](#)), ML16 was the first study that specifically targeted the AGB to investigate stellar evolution using the multiple population phenomenon of M 4.

Due to the controversial nature of the discovery of ML16, and uncertainties regarding the separation of the sub-populations in $[\text{Na}/\text{O}]$ space, caveats to the conclusions arising from the study were noted. M 4 is a moderately metal-poor ($[\text{Fe}/\text{H}] = -1.16$; [Harris 1996](#)) cluster that displays a distinctly bimodal HB ([Marino et al. 2011](#)) and a well established Na-O anti-correlation on the RGB and HB. While M 4 does not exhibit a Mg-Al anti-correlation (Mg has been observed to be homogeneous in M 4), Al correlates with Na ([Marino et al. 2008](#)).

The conclusions of ML16 motivated the publication of three additional studies (to date) of AGB stars in M 4 by three separate research groups. Using the photometric index C_{UBI} (which has been shown to correlate with light-elemental abundances in RGB stars; [Monelli et al. 2013](#)), [Lardo et al. \(2017\)](#) determined the spread in C_{UBI} values to be quantitatively similar between the AGB and RGB in M 4, in contradiction to the spectroscopic findings of ML16. Using high-resolution spectra, [Marino et al. \(2017, hereafter Mar17\)](#) came to the same conclusion as [Lardo et al. \(2017\)](#) by showing that a sample of 17 AGB stars had a similar range in $[\text{Na}/\text{Fe}]$ values as the RGB sample from [Marino et al. \(2008, hereafter Mar08\)](#). However, with similar data, [Wang et al. \(2017, hereafter W17\)](#) found that M 4 AGB stars have lower $[\text{Na}/\text{H}]$ values than stars on the RGB, and that the most Na-rich stars did appear to be missing from the AGB, but not to the extreme degree that ML16 had concluded. Thus a significant uncertainty exists within the literature with regard to the nature of M 4’s AGB population.

The mixed and contradictory results of recent studies into the light-elemental abundances of M 4’s AGB population call for a detailed, quantitative reinvestigation of the available data in order to identify why the results differ. In this paper we adopt the \mathcal{F} parametrisation of SP2 AGB deficits¹ that was used in ML16 and [MacLean et al. \(2018, hereafter ML18a\)](#).

This paper is structured as follows. In Section 2 we re-analyse our previously published sample of high-resolution M 4 stellar spectra in order to test the robustness of our earlier study on M 4 (ML16). In Section 3 we calculate CN band strengths from previously unpublished low-resolution spectra of M 4 stars. In an attempt to resolve the conflicting conclusions in recent (and historical) spectroscopic studies, we compare our abundance and CN results with M 4 AGB and RGB data from the literature in Section 4. In Section 5 we use 1D stellar evolution models to establish a precise, quantitative theoretical expectation of the abundance distribution of the AGB of M 4. In Section 6 we investigate possible explanations for the AGB results found in this study (and throughout the literature) including a series of tests

¹ $\mathcal{F} = (1 - \frac{\mathcal{R}_{\text{AGB}}}{\mathcal{R}_{\text{RGB}}}) \cdot 100\%$, where the percentages of RGB and AGB stars in a GC that are found to be members of SP2 are written as \mathcal{R}_{RGB} and \mathcal{R}_{AGB} . For example, [Campbell et al. \(2013\)](#) reported $\mathcal{R}_{\text{RGB}} = 70\%$ and $\mathcal{R}_{\text{AGB}} = 0\%$ for NGC 6752.

utilising a range of stellar atmospheric models. Finally, we summarise our results and conclusions in Section 7.

2 HIGH-RESOLUTION SPECTRA RE-ANALYSIS

In order to be confident in our earlier results, which have been challenged in the literature, we re-analysed our sample of M4 stellar spectra upon which our ML16 results were based. The motivation behind this re-analysis was to i) check the ML16 results in light of recent debate on stellar parameter determination for AGB stars in GCs (see Lapenna et al. 2016; Campbell et al. 2017), and ii) increase the number of elements available for use as a diagnostic of multiple populations. Specifically, we redetermined the stellar parameters (T_{eff} , v_t , $\log g$, and $[\text{Fe}/\text{H}]$) and abundances (Na and O) that were published in ML16. We also determined abundances of Mg and Al for our full sample of 15 AGB and 106 RGB stars.

2.1 Targets and data

The reduced M4 high-resolution spectra and photometry used in this study are the same as those used in ML16. M4 suffers from significant differential reddening, however constant reddening values were used in ML16. Here we improve upon this, with each star corrected using the reddening map of Hendricks et al. (2012). Individual corrections are included in Table 1. We found an average reddening value of $E(B-V) = 0.37$ and a 1σ star-to-star scatter of ± 0.02 . This differential reddening map, however, does not cover our entire sample, and some stars were only adjusted according to the average reddening value.

The M4 targets included in this study are presented in Figure 1. In total, 24 AGB stars were identified in the photometry of Momany et al. (2003). Seven of these were not observable due to 2dF fibre positioning restrictions, and two were found in ML16 to be non-members, leaving a final sample of 15. Due to the randomness of stellar astrometry within a GC, we did not identify any sources of selection bias.

2.2 Atmospheric parameters

For the determination of surface gravity ($\log g$), we did not adopt the standard spectroscopic approach, wherein ionisation balance between abundances determined from neutral and singly-ionised Fe lines is enforced. This is because such an approach can be biased by not accounting for non-LTE effects on Fe I lines (Ivans et al. 1999; Lapenna et al. 2016; Sitnova et al. 2015). Therefore, we instead calculated $\log g$ using estimates of T_{eff} , luminosity and mass. The luminosity was computed from de-reddened V magnitudes, with bolometric corrections from Alonso et al. (1999). We assumed a mass of $0.8 M_{\odot}$ and $0.7 M_{\odot}$ for the RGB and AGB, respectively (Miglio et al. 2016).

We investigated different approaches to determining the effective temperatures (T_{eff}) of our stars. T_{eff} determinations can be subject to significant uncertainties, both random and systematic. Incorrect modelling assumptions, and

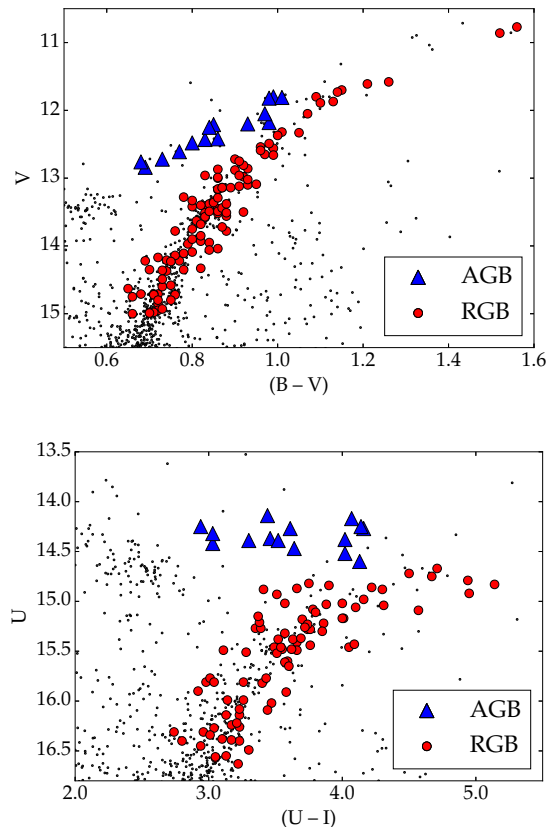


Figure 1. $V - (B - V)$ and $U - (U - I)$ colour-magnitude diagrams of M4 RGB and AGB target stars, displayed over the full photometric sample of Momany et al. (2003, black points). In the top panel, targets have been corrected for extinction according to the differential reddening map of Hendricks et al. (2012), and a constant value of $(B - V) = 0.37$ was applied to the non-target photometric data. No reddening correction has been applied to the $(U - I)$ photometry in the bottom panel.

degeneracies in the stellar spectra with respect to different stellar parameters, can lead the standard spectroscopic method (requiring a balance of line-by-line Fe I abundances over a range of excitation potentials) to give unreliable and/or significantly offset T_{eff} values. Similarly, the photometric method (utilising empirical relations between T_{eff} and photometric magnitudes) can potentially produce large uncertainties (up to ± 200 K); for example, see Campbell et al. (2017, C17) for a detailed investigation of T_{eff} determination using the photometric method, and its effect on Fe and Na abundances determined for AGB and RGB stars.

Due to i) the high level of differential reddening in M4 (and the fact that our sample is not fully covered by the reddening map of Hendricks et al. 2012), and ii) the debate within the literature as to appropriate selections of colour- T_{eff} empirical relationships (see C17), we endeavoured to further improve the spectroscopic T_{eff} determination from our spectroscopic code PHOBOS. Version one of this code (PHOBOS v1) was used in ML16 to determine parameters spectroscopically, but it was dependent on having accurate initial photometric estimates of T_{eff} . In C17 we noted that spectroscopic codes and methods appear to give effective temperatures that inherit some of the biases/trends

Table 1. M4 target details including data from Momany et al. (2003, *UBVI* photometry and target IDs) and 2MASS (Skrutskie et al. 2006, *JHK* photometry), and differential reddening corrections. Gaps in 2MASS data represent targets with low quality flags. Stars for which no reddening value is listed were outside the reddening map of Hendricks et al. (2012), and were corrected according to the average reddening value of $E(B - V) = 0.37$. Only the first five rows are shown; the full table is available online.

ID	Type	2MASS ID	<i>V</i>	<i>B</i>	<i>U</i>	<i>I</i>	<i>J</i>	<i>H</i>	<i>K</i>	$E(B - V)$
788	AGB	16235772-2622557	12.21	13.43	14.14	10.69	9.64	9.00	8.82	-
3590	AGB	16232184-2630495	12.48	13.64	14.37	10.92	-	-	-	0.36
10092	AGB	16233067-2629390	12.61	13.74	14.39	11.09	-	-	-	0.36
11285	AGB	16233195-2631457	12.84	13.90	14.42	11.40	10.35	9.77	9.58	0.37
13609	AGB	16233477-2631349	12.76	13.81	14.25	11.31	10.21	9.65	9.48	-
⋮	⋮	⋮	⋮	⋮	⋮	⋮	⋮	⋮	⋮	⋮

in colour- T_{eff} relations (see §4 in C17). We investigated this problem in PHOBOS v1 and found that, in our case, this bias was due to the choice of the numerical scheme employed to iterate to a solution.

In principle, the choice of photometric estimate should have no bearing on the spectroscopic parameters that the code determines – that is, the spectroscopic parameters should only be a function of the Fe absorption line-list, and not the initial photometric estimates. We have improved the numerical scheme in PHOBOS v2 to search for global minima in the stellar parameter space, so that the initial T_{eff} estimates only require an accuracy of ~ 1000 K, and so that the code is ‘agnostic’ about the initial T_{eff} estimate. PHOBOS v2 determines T_{eff} by requiring no trend between the excitation potential of Fe I absorption lines and the abundances calculated from those lines. Initial microturbulence (v_t) estimates were determined using the empirical relation from Gratton et al. (1996), while final spectroscopic values are required to have no trend between the reduced wavelength of Fe I lines and their associated line-by-line abundances.

To test the efficacy of our improved code (PHOBOS v2), we conducted two tests, using our entire M4 sample of 121 giant stars, to determine spectroscopic parameters primarily based on two very different sets of photometrically estimated initial-guess T_{eff} values. The first set of initial guesses ($T_{\text{eff,ph}}$) are an average of six predictions from the empirical $B - V$ and $V - K$ relations of Ramírez & Meléndez (2005), González Hernández & Bonifacio (2009), and Casagrande et al. (2010), and one direct calculation by implementing the infrared flux method (IRFM) at an estimated $\log g$ of each star using *BVI* and 2MASS *JHK* photometry (Casagrande et al. 2014). For stars that were flagged for low quality and/or contamination in the 2MASS database, only the $B - V$ relations were used to determine $T_{\text{eff,ph}}$, while for all other stars, the mean of the seven estimates was adopted as $T_{\text{eff,ph}}$. These methods are mildly dependent on metallicity, for which a value of $[\text{Fe}/\text{H}] = -1.10$ was assumed (a change in adopted metallicity of 0.1 dex alters $T_{\text{eff,ph}}$ values by ~ 10 K). Table 2 summarises the average difference between the adopted $T_{\text{eff,ph}}$ values and those of the individual photometric relations and IRFM – the systematic differences between the relations highlight that individual photometric relations are often poor choices for determining stellar parameters. Individual $T_{\text{eff,ph}}$ values are listed in Table 3. For the second, and extreme, test of PHOBOS v2, the initial T_{eff} guesses of every star (regardless of evolutionary phase) were assumed to be identical: $T_{\text{eff}} = 4500$ K, $\log g = 2.5$,

Table 2. Average differences between the average $T_{\text{eff,ph}}$ values and each photometric estimate ($T_{\text{eff,ph}} - T_{\text{eff,estimate}}$) for our first PHOBOS test. Uncertainties are the standard deviations of the stellar sample, with the quoted uncertainty of each relation in brackets (except for IRFM, which is the average IRFM uncertainty of our sample).

Method	ΔT_{eff} (K)
Ram ($B - V$) ¹	0 ± 71 (51)
Gonz ($B - V$) ²	-49 ± 70 (57)
Casa ($B - V$) ³	-74 ± 89 (73)
Ram ($V - K$)	132 ± 52 (28)
Gonz ($V - K$)	24 ± 48 (23)
Casa ($V - K$)	-2 ± 54 (25)
IRFM ³	-5 ± 62 (33)
Average σ	64

¹Ramírez & Meléndez (2005)

²González Hernández & Bonifacio (2009)

³Casagrande et al. (2010)

and $v_t = 1.5$ – broadly representative of a giant GC star. We designate this second set of initial guesses as $T_{\text{eff,4500}}$.

We used PHOBOS v2 to determine spectroscopic parameters twice, once using the parameter set $T_{\text{eff,ph}}$, and again using the $T_{\text{eff,4500}}$ set of parameters for the initial guess. As seen in Figure 2, the differences between the spectroscopically determined effective temperature values using the two different initial estimates ($T_{\text{eff,sp,ph}}$ and $T_{\text{eff,sp,4500}}$) are extremely small, with $\Delta T_{\text{eff}} = 0 \pm 2$ K, while the the average difference between the photometric ($T_{\text{eff,ph}}$) and spectroscopic ($T_{\text{eff,sp}}$) values is $\Delta T_{\text{eff}} = 12 \pm 76$ K. This indicates that no information from the photometric T_{eff} estimates is retained within the spectroscopic results. This is beneficial because the final stellar parameters are independent of the choice of colour- T_{eff} relation, and are therefore reproducible and consistent.

In summary, we adopt the spectroscopic parameters included in Table 3 and presented in Figure 3. The subsequent elemental abundance determinations were based on these stellar parameters. PHOBOS v2 now also calculates star-to-star T_{eff} and v_t uncertainties based on the standard error of the slope between excitation potential and reduced wavelength, and line-to-line Fe I abundances. These uncertainties are included in Table 3. The typical 1σ T_{eff} and v_t uncertainties of our sample are 65 K and 0.1 km/s, respectively, and we adopt a 1σ $\log g$ uncertainty of 0.2 dex.

Table 3. Stellar parameters for each star in our M4 sample. Spectroscopic effective temperatures ($T_{\text{eff,sp}}$), microturbulence values (v_t), and uncertainties were determined using PHOBOS v2, while $\log g$ values were calculated based on the empirical relation from [Alonso et al. \(1999\)](#). These were adopted as our final parameters. $T_{\text{eff,ph}}$ values are the effective temperatures estimated from photometric colour- T_{eff} relations, were used in the PHOBOS test, and are included for comparison (also see Figure 2). Only the first five rows are shown; the full table is available online.

Star ID	Evolutionary phase	$T_{\text{eff,sp}}$ (K)	$\log g$ (cgs)	v_t (km/s)	$T_{\text{eff,ph}}$ (K)
788	AGB	4877 ± 52	1.71	1.56 ± 0.07	4937
3590	AGB	4929 ± 36	1.84	1.68 ± 0.06	4975
10092	AGB	4944 ± 29	1.90	1.45 ± 0.04	5051
11285	AGB	5137 ± 69	2.08	1.73 ± 0.19	5154
13609	AGB	5131 ± 67	2.05	1.21 ± 0.10	5166
\vdots	\vdots	\vdots	\vdots	\vdots	\vdots

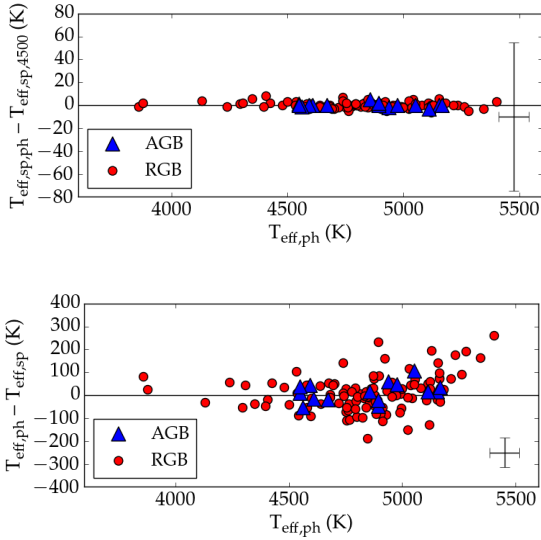


Figure 2. **Top panel:** The star-to-star differences between the spectroscopic $T_{\text{eff,sp}}$ values determined (using PHOBOS v2) based on initial estimates from i) photometrically estimated stellar parameters ($T_{\text{eff,ph}}$), and ii) a single T_{eff} of 4500 K ($T_{\text{eff},4500}$). The average difference between the spectroscopic values of the two tests is $\Delta T_{\text{eff}} = 0 \pm 2$ K. **Bottom panel:** The star-to-star differences between our photometrically estimated $T_{\text{eff,ph}}$ values and final adopted spectroscopic $T_{\text{eff,sp}}$ values. Error bars in both panels are our typical $T_{\text{eff,sp}}$ uncertainties ~ 65 K, as determined by PHOBOS v2 (see text for more detail).

2.3 Chemical abundance determination

With our improved stellar parameters, we adopted the method of [ML18a](#) for the determination of chemical abundances. This is mostly the same as the method previously used for this sample ([ML16](#)), but with an updated line list (that includes Mg and Al) and non-LTE corrections from more recent sources where available. In brief, the equivalent width (EW) method was used in combination with the ARES ([Sousa et al. 2015, v2](#)), IRAF *onedspec*, and MOOG ([Sneden 1973](#), June 2014 release) packages, with α -enhanced (+0.4 dex) 1D model atmospheres interpolated from the [Castelli & Kurucz \(2004\)](#) grid. Although the M4 spectral data is unchanged from [ML16](#), for consistency all Na I and

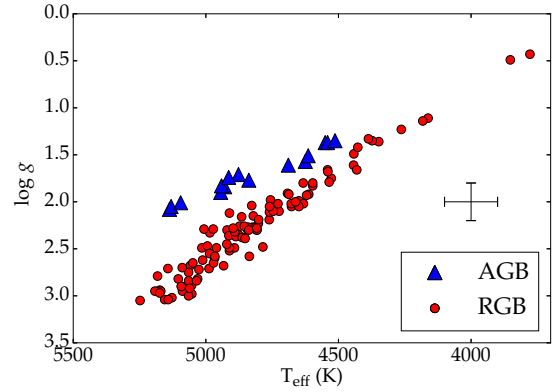


Figure 3. Final T_{eff} and $\log g$ values of our M4 stellar sample, determined spectroscopically using PHOBOS v2. Typical uncertainties are indicated (see Table 6).

O I EWs were remeasured (with little change), while Mg I, and Al I EWs are new, since these abundances were not determined in [ML16](#).

All absorption lines measured are known to suffer from non-LTE effects ([Bergemann & Nordlander 2014](#)). Abundances of O, Na, and Al were corrected for these non-LTE effects by interpolation of the grids from [Amarsi et al. \(2016a, O\)](#), [Lind et al. \(2011, Na\)](#), and [Nordlander & Lind \(2017, Al\)](#). Mg was not corrected for non-LTE because it is known (and confirmed in this study) to be homogeneous in M4. More detail of this method, and our adopted line list, can be found in [ML18a](#).

As in [ML18a](#), we were unable to correct our derived Fe abundances for non-LTE effects on a line-by-line basis due to the large number of Fe I lines in the stellar spectrum. We have therefore performed a test on a representative subset of three RGB and three AGB stars from M4, using corrections interpolated from the [Amarsi et al. \(2016b\)](#) grid for five Fe I lines² and two Fe II lines³. For our sample of M4 stars the non-LTE effects on Fe I and Fe II are negligible considering our uncertainty in individual abundances (discussed in §2.4), thus we do not apply them to our final abundances. The

² 4788.8Å, 4839.5Å, 5701.6Å, 5753.1Å and 7748.3Å

³ 6516.1Å and 7711.7Å

Table 4. Summary of average non-LTE corrections for each chemical species.

Species	Average non-LTE Correction	
	AGB	RGB
Fe I	+0.00 ± 0.03	-0.01 ± 0.07
Fe II	-0.01 ± 0.00	-0.01 ± 0.01
O I	-0.16 ± 0.04	-0.10 ± 0.02
Na I	-0.11 ± 0.03	-0.14 ± 0.03
Al I	-0.13 ± 0.03	-0.10 ± 0.03

O, Na, Al non-LTE corrections for our sample are largely systematic with minimal star-to-star scatter. However, the average corrections for the three species are slightly different ($\Delta_{\text{corr}} \sim 0.03$ to 0.06) for the AGB and RGB. We summarise the results of our Fe non-LTE test along with the non-LTE corrections of Na and Al abundances in Table 4.

2.4 Abundance results

Chemical abundances using the new stellar parameters from this study are presented in Table 5. Individual uncertainties cited in these tables are based only on the line-to-line scatter of each abundance. Using the 1σ uncertainties of each stellar parameter (± 65 K in T_{eff} , ± 0.2 in $\log g$, ± 0.1 km/s in v_t), an atmospheric sensitivity analysis was performed on a representative sub-sample and the results are summarised in Table 6. The uncertainty in abundances due to atmospheric uncertainties is $\leq \pm 0.05$ for all species, except for Fe II and O I which are ± 0.10 and ± 0.13 , respectively.

The use of elemental ratios with respect to Fe can be problematic, especially in globular clusters that are homogeneous in Fe abundance at the level of uncertainty in the relevant studies (i.e. when not using differential analysis methods such as in [Yong et al. 2013](#)). In these cases, dividing star-to-star elemental abundances by Fe abundance adds noise from the imperfect measurement of $[\text{Fe}/\text{H}]$ and thereby degrades the signal in star-to-star abundance distributions (see [C17](#) for a detailed analysis). Throughout this paper we present all abundances in the form $\log_{\epsilon}(X)$ ⁴, which eliminates many systematic offsets that may exist in $[\text{X}/\text{Fe}]$ and $[\text{X}/\text{H}]$ ratios – for example adopted solar abundances, and the sensitivity of Fe I to T_{eff} .

A detailed comparison to recent high-resolution spectroscopic studies of M 4 is not only warranted, but crucial for this cluster. We reserve this analysis and discussion for §4, except for a comparison with our previous results ([ML16](#)), which is presented in Table 8. The only change of note is in $\log g$. In [ML16](#) we assumed a mass of $0.8 M_{\odot}$ for all stars, while here we assumed a mass of $0.7 M_{\odot}$ for our AGB sample, which accounts for -0.10 dex of the -0.15 difference in $\log g$ values for the AGB stars. No other significant changes occurred in the re-analysis, with T_{eff} , $\log_{\epsilon}(\text{Fe I})$, $\log_{\epsilon}(\text{O})$, and $\log_{\epsilon}(\text{Na})$ showing very little change. The scatter is indicative

⁴ $\log_{\epsilon}(X) = \log_{10}(N_X/N_H) + 12.0$, where N_X represents the number density of atoms of element X .

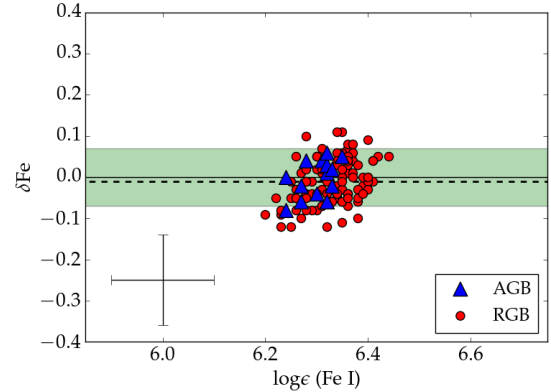


Figure 4. Fe abundances for this study. Here, ionisation difference ($\delta\text{Fe} = \log_{\epsilon}(\text{Fe I}) - \log_{\epsilon}(\text{Fe II})$) is plotted against $\log_{\epsilon}(\text{Fe I})$ abundance to highlight departures from LTE in Fe I, and the similarity between the Fe abundances of the AGB and RGB. The error bar indicates typical 1σ total uncertainties in individual abundances (i.e. the line-to-line uncertainties and the 1σ atmospheric sensitivity uncertainties added in quadrature), while the black dashed line represents the sample average δFe value of -0.01 . The shaded green region indicates the non-LTE uncertainties quoted in [Amarsi et al. \(2016b\)](#), ± 0.05 dex, around the expected δFe value ($+0.00$ dex, solid black line) from our non-LTE test (see §2.3).

of our parameter uncertainties⁵ and estimated total abundance errors (Table 7).

Abundances from Fe II lines were not published in [ML16](#), but are included here as part of our re-analysis. In Figure 4 we plot $\log_{\epsilon}(\text{Fe I})$ against δFe (ionisation balance; $\delta\text{Fe} = \log_{\epsilon}(\text{Fe I}) - \log_{\epsilon}(\text{Fe II})$). Our non-LTE test (see §2.3) predicted a theoretical δFe value of 0.00 ± 0.07 , while our observed sample has an average δFe of -0.01 ± 0.05 . This high level of agreement is strong evidence that our PHOBOS v2 spectroscopic method is reliable, and that our stellar parameters are accurate.

As in [ML16](#), M 4 shows a significant spread in Na abundance among RGB stars ($\sigma = \pm 0.19$ dex; see Figure 5). However, considering the uncertainty in O abundance we cannot resolve the Na-O anti-correlation that has been reported elsewhere (e.g. [Marino et al. 2008](#)). In fact, given the total uncertainty in our O abundances of ± 0.15 dex (Table 7) – compared to the O spread on the RGB of ± 0.12 dex (Table 5) – we cannot say that M 4 actually shows heterogeneity in O abundance, formally it appears to be homogeneous. This uncertainty in $\log_{\epsilon}(\text{O})$ comes from the large sensitivity of the 777nm triplet to T_{eff} and $\log g$, and is typically smaller for other O lines that we could not observe with HERMES/AAT. Na, on the other hand, shows a significant star-to-star scatter in both the RGB, and (to a smaller degree; $\sigma = \pm 0.12$ dex) the AGB.

We find a correlation between Na and Al abundance, but no evidence of a Mg-Al anti-correlation (Figure 6), in agreement with previous results (e.g. [Mar08](#)). A clear outlier is the star AGB18573 which appears to have a low Na abun-

⁵ An exception is the scatter in v_t differences, which has little effect on elemental abundances – see Table 6.

Table 5. Chemical abundances for each star in our M4 sample. Abundance uncertainties reflect line-to-line scatter (1σ), and do not take atmospheric sensitivities into account (see Table 6). The last four lines show the cluster average abundances (for the AGB and RGB) with standard error of the mean, and standard deviation to indicate observed scatter. O, Na, and Al abundances were corrected for non-LTE effects. Only the first five rows are shown; the full table is available online.

ID	Type	$\log_\epsilon(\text{Fe I})$	$\log_\epsilon(\text{Fe II})$	$\log_\epsilon(\text{O})$	$\log_\epsilon(\text{Na})$	$\log_\epsilon(\text{Mg})$	$\log_\epsilon(\text{Al})$
788	AGB	6.24 ± 0.08	6.24 ± 0.03	8.26 ± 0.05	4.93 ± 0.01	6.79 ± 0.03	5.56 ± 0.02
3590	AGB	6.27 ± 0.06	6.29 ± 0.04	8.07 ± 0.01	5.15 ± 0.03	6.73 ± 0.04	5.67 ± 0.03
10092	AGB	6.33 ± 0.04	6.35 ± 0.01	8.29 ± 0.06	4.95 ± 0.02	6.72 ± 0.03	5.53 ± 0.03
11285	AGB	6.32 ± 0.07	6.31 ± 0.04	8.10 ± 0.04	5.19 ± 0.02	6.80 ± 0.02	5.71 ± 0.06
13609	AGB	6.32 ± 0.09	6.38 ± 0.06	8.12 ± 0.04	5.02 ± 0.11	6.76 ± 0.05	5.57 ± 0.05
\vdots	\vdots	\vdots	\vdots	\vdots	\vdots	\vdots	\vdots
Mean	AGB	6.30 ± 0.01	6.31 ± 0.01	8.18 ± 0.02	5.11 ± 0.03	6.76 ± 0.01	5.62 ± 0.02
σ		0.03	0.04	0.09	0.12	0.03	0.08
Mean	RGB	6.33 ± 0.01	6.34 ± 0.01	8.10 ± 0.01	5.33 ± 0.02	6.78 ± 0.01	5.76 ± 0.01
σ		0.05	0.06	0.12	0.19	0.05	0.09

Table 6. Typical abundance uncertainties due to the (1σ) atmospheric sensitivities of a representative sub-sample of three RGB and two AGB stars in our M4 data set. Parameter variations (in parentheses) are the adopted uncertainties in the respective parameters. Note the direction of signs.

	ΔT_{eff} (± 65 K)	$\Delta \log g$ (± 0.2)	Δv_t (± 0.1)	Total
$\log_\epsilon(\text{Fe I})$	± 0.05	± 0.00	∓ 0.02	± 0.05
$\log_\epsilon(\text{Fe II})$	∓ 0.05	± 0.09	∓ 0.02	± 0.10
$\log_\epsilon(\text{O})$	∓ 0.10	± 0.08	∓ 0.01	± 0.13
$\log_\epsilon(\text{Na})$	± 0.05	∓ 0.01	∓ 0.02	± 0.04
$\log_\epsilon(\text{Mg})$	± 0.03	± 0.00	∓ 0.01	± 0.03
$\log_\epsilon(\text{Al})$	± 0.04	± 0.00	± 0.00	± 0.04

Table 7. Summary of typical abundance uncertainties (1σ) from each source identified in the text, and the total uncertainties (when added in quadrature). The first column are the average line-to-line uncertainties of all stars, values in the second column are the total uncertainties from atmospheric sensitivities (Table 6), and the third column represents the typical uncertainties in non-LTE corrections, as reported in the relevant sources (see §2.3). Note that individual Fe abundances were not corrected for non-LTE (see text for details).

Species	Line-to-Line	Atmospheric	non-LTE	Total
Fe I	± 0.09	± 0.05	-	± 0.10
Fe II	± 0.04	± 0.10	-	± 0.11
O	± 0.05	± 0.13	± 0.05	± 0.15
Na	± 0.04	± 0.04	± 0.04	± 0.07
Mg	± 0.04	± 0.03	-	± 0.05
Al	± 0.03	± 0.04	± 0.06	± 0.08

dance but a high Al abundance. We have not been able to provide an explanation for this anomalous star, however, it was reported by Mar17 to be similarly Na-poor and Al-rich. We find Mg to be homogeneous in M4 ($\sigma = \pm 0.05$ dex on the RGB), while Al is difficult to classify because the star-to-star scatter ($\sigma = \pm 0.09$ and ± 0.08 dex on the RGB and AGB, respectively) is similar to our total uncertainties in the abundance (± 0.08 dex). We note however, that for the

Table 8. The average differences in parameters and abundances between this study and MacLean et al. (2016, ML16). Uncertainties are standard deviations, and indicate the scatter between the studies, if the offsets were removed. The significant change in $\log g$ values is discussed in the text. Note that abundances from Fe II lines were not published in ML16.

Parameter	This study – ML16 (AGB)	(RGB)
ΔT_{eff}	-21 ± 44	-20 ± 57
$\Delta \log g$	-0.15 ± 0.12	-0.04 ± 0.10
Δv_t	$+0.12 \pm 0.18$	$+0.12 \pm 0.15$
$\Delta \log_\epsilon(\text{Fe I})$	-0.02 ± 0.04	-0.02 ± 0.05
$\Delta \log_\epsilon(\text{O})$	$+0.06 \pm 0.07$	$+0.04 \pm 0.09$
$\Delta \log_\epsilon(\text{Na})$	-0.03 ± 0.06	$+0.00 \pm 0.06$

AGB, the 1σ spread in Al abundance reduces to ± 0.06 dex when the Al-rich outlier AGB18573 is discounted, and can be seen in Figure 6 to have a smaller spread than our RGB sample.

As in ML16, the average Na, O, and Al abundances of AGB stars in M4 are clearly different to that of the RGB, being heavily weighted toward SP1-like abundances. Our Fe and Mg abundances are constant, and the average RGB and AGB abundances agree. These results are consistent with our claim in ML16 that M4 may not contain SP2 AGB stars ($\mathcal{F} = 100\%$). Due to the spread in AGB Na abundances, and our abundance uncertainties, we conclude that $\mathcal{F} \gtrsim 65\%$ – i.e. less than 20% of AGB stars, or 3 out of 15, have SP2-like abundances. This compares with 55% on the RGB. This value is considerably higher than that expected from stellar evolutionary theory ($\mathcal{F} = 0\%$) for a cluster with a HB extending only to $T_{\text{eff}} \simeq 9000$ K.

3 CYANOGEN BAND STRENGTHS FROM LOW-RESOLUTION SPECTRA

As a further observational check of the relative abundance distributions of M4’s AGB and RGB, we determined CN band-strengths for a sample of M4 stars. The bimodality of CN band strengths in M4 is well established (Norris 1981;

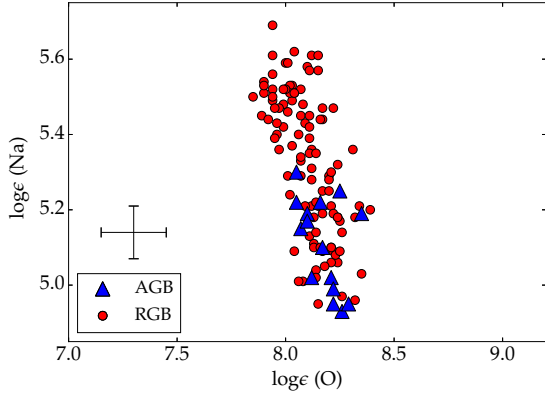


Figure 5. O and Na abundances for our M4 sample. The error bar indicates typical 1σ total uncertainties in individual abundances (i.e. the line-to-line uncertainties and the 1σ atmospheric sensitivity uncertainties added in quadrature).

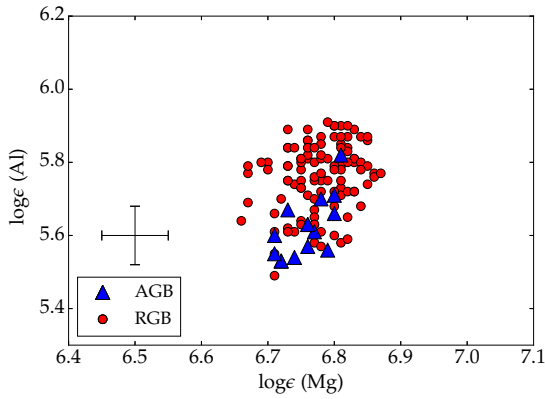


Figure 6. Same as Figure 5, but for Mg and Al abundances.

Ivans et al. 1999), and can be used to identify to which subpopulation (SP1 or SP2) a star belongs because CN band strengths have been shown to correlate with Na abundance⁶ (Cottrell & Da Costa 1981; Campbell et al. 2012; Smith 2015).

In addition to our sample of high-resolution spectra, low-resolution spectra of M4 stars were collected in September 2009 (Campbell et al. 2010) using the AAOmega/2dF multi-object spectrograph on the Anglo-Australian Telescope ($R \simeq 3000$; Lewis et al. 2002; Saunders et al. 2004; Sharp et al. 2006). We used the 1700B grating which gave a spectral coverage from 3755 Å to 4437 Å, while the signal-to-noise ratio for all targets was $\gtrsim 20$. The software package 2DFDR (AAO Software Team 2015, v3.211) was used to reduce the data in preparation for analysis. This is new and unpublished data, and is included to provide an additional avenue for the investigation of M4 abundance distributions. A total of 7 AGB and 19 RGB stars were observed with

⁶ CN band strengths are primarily indicative of atmospheric N abundance, which correlates with Na

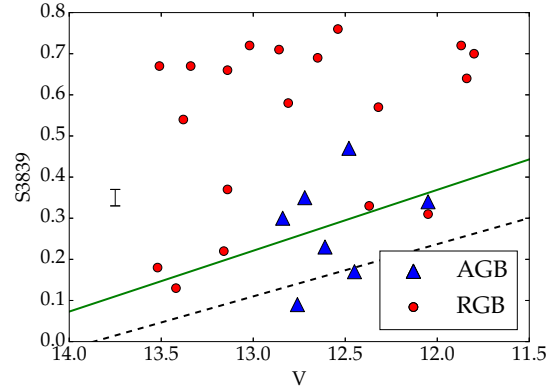


Figure 7. S3839 CN index values versus V-band magnitudes for our M4 low-resolution sample. The green trend-line is a linear best fit for the five RGB stars with the lowest CN band strengths ($S3839 = -0.148V + 2.145$), while the dashed trend-line is the baseline from Figure 3 of Norris (1981, $S3839 = -0.127V + 1.761$). The typical S3839 uncertainty is represented on the left.

AAOmega; all but two of which (stars 25133 and 17999) were included in our HERMES target list.

To quantify the CN band strengths we use the S3839 CN index from Norris (1981) which compares a spectral segment where the CN molecule absorbs light with a neighbouring pseudo-continuum:

$$S3839 = -2.5 \log \frac{\int_{3846}^{3883} I_{\lambda} d\lambda}{\int_{3883}^{3916} I_{\lambda} d\lambda}. \quad (1)$$

IRAF was used to measure the integrated fluxes of our low-resolution spectra. Target data, S3839 values, and $\delta S3839$ excess values are given in Table 9. CN band strengths are presented in Figure 7.

Even without adjusting for the trend with V band magnitude (called the baseline in Norris 1981; Ivans et al. 1999), it can be seen that the RGB stars display a significant spread in S3839 values, and that our AGB sample are heavily weighted to low S3839 index values. The green fiducial line in Figure 7 was used to empirically correct for the trend between V band magnitude and S3839 value ($\delta S3839$ excess is the vertical distance of each star to the green fiducial), and as a reference we include the baseline used by Norris (1981) which is qualitatively similar.

We adopt the characteristic S3839 uncertainty of ± 0.02 from Campbell et al. (2012), which was based on the typical differences between S3839 measurements from two separate observations of the same star in the GC NGC 1851 (the spectra of which were obtained during the same observing program and with the same technical specifications as the M4 spectra used in this study), and a typical $\delta S3839$ uncertainty of 0.08 dex due to assumptions in determining the trend with V band magnitude. We discuss our CN results further in the next section, in comparison with previous CN studies on M4.

Table 9. S3839 CN index values for the low-resolution M4 sample, along with V -band magnitudes and $\delta S3839$ excess values. The last four lines show the cluster average abundances (for the AGB and RGB) with standard error of the mean, and standard deviation to indicate observed scatter. Note that all but two (stars 25133 and 17999) of the low-resolution targets were also observed with HERMES in high-resolution. V -band magnitudes and IDs are from Momany et al. (2003).

ID	Type	V	S3839	$\delta S3839$
3590	AGB	12.48	0.47	0.17
10092	AGB	12.61	0.23	-0.04
11285	AGB	12.84	0.30	0.06
13609	AGB	12.76	0.09	-0.17
20089	AGB	12.72	0.35	0.05
25133	AGB	12.45	0.17	-0.13
46676	AGB	12.05	0.34	-0.02
1029	RGB	13.14	0.66	0.46
3114	RGB	13.38	0.54	0.37
4361	RGB	13.51	0.67	0.52
4806	RGB	13.16	0.22	0.03
4938	RGB	12.86	0.71	0.46
6978	RGB	13.34	0.67	0.50
7298	RGB	13.42	0.13	-0.03
8803	RGB	11.87	0.72	0.34
9040	RGB	12.32	0.57	0.25
10801	RGB	12.54	0.76	0.45
10928	RGB	11.80	0.70	0.30
12387	RGB	13.14	0.37	0.17
13170	RGB	13.52	0.18	0.04
14037	RGB	12.05	0.31	-0.05
14350	RGB	12.65	0.69	0.42
14377	RGB	12.81	0.58	0.33
15010	RGB	12.37	0.33	0.01
17999	RGB	11.84	0.64	0.24
23196	RGB	13.02	0.72	0.50
Mean	AGB	-	0.28 ± 0.03	-0.01 ± 0.03
σ			0.13	0.12
Mean	RGB	-	0.51 ± 0.02	0.23 ± 0.02
σ			0.21	0.25

4 LITERATURE COMPARISON OF AGB ABUNDANCES

After determining reliable elemental abundances and CN band strengths, we compiled and compared spectroscopic results from the literature in order to investigate the conflicting conclusions regarding M4’s AGB abundances.

While ML16 was the first study that systematically targeted the AGB of M4, AGB stars had been included previously in several spectroscopic studies of the cluster: Norris (1981), Suntzeff & Smith (1991), and Ivans et al. (1999, hereafter I99). CN band strengths and abundances from these three studies were compiled and merged into the data set of Smith & Briley (2005, hereafter SB05) who reported on six AGB stars (two of which they classified as CN-strong, one as CN-intermediate, and the remaining three as CN-weak). I99 reported that their AGB abundances show less evidence of H-burning than their RGB sample, and described their AGB results as “puzzling”.

Soon after the publication of ML16, Lardo et al. (2017) disputed our conclusion by utilising a pseudo-CMD with the photometric index $C_{UBI} = (U - B) - (B - I)$, which

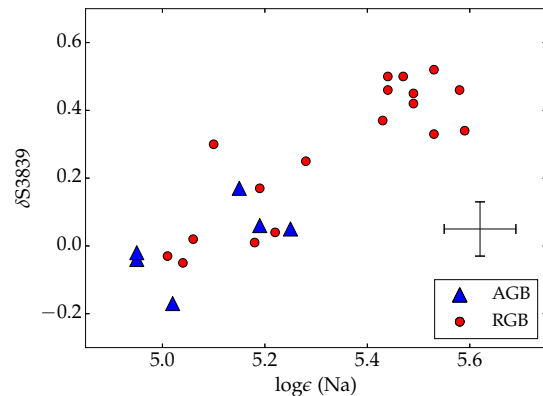


Figure 8. $\delta S3839$ (excess CN index values) versus Na abundances for stars in both our M4 HERMES and AAOmega samples. $\delta S3839$ values are the distance a star is above the green trend-line in Figure 7. The error bar represents typical uncertainties. Note that for two stars (25133 and 17999) only low-resolution spectra were observed, and they are therefore not included in this plot.

has been used to separate the RGB (and the AGB more recently) subpopulations of GCs (e.g. Monelli et al. 2013; García-Hernández et al. 2015). They demonstrated that the spread in C_{UBI} for their sample of AGB stars is statistically similar to that of the RGB. Mar17 performed a similar study using both the C_{UBI} index and the combination of Hubble Space Telescope (HST) filters $C_{F275W, F336W, F438W} = (m_{F275W} - m_{F336W}) - (m_{F336W} - m_{F438W})$. They came to a similar conclusion as Lardo et al. (2017) – that photometric data of M4 stars suggest that both SP1 and SP2 stars ascend the AGB. Evidence for this lies in the broadness of the branches in the pseudo-CMDs, for which a double sequence (or a single sequence that is broader than expected from observational errors) is understood to indicate a spread in the abundances of H-burning products (primarily He, N, and C; see Milone et al. 2012). Both photometric investigations of the AGB of M4 found that the broadness of the branch is consistent with a heterogeneity in He, N, and C of similar magnitude as the RGB of M4, in contradiction to the conclusions of ML16.

Although C_{UBI} has been used to infer most of these results, the broadness of the UBI filter pass-bands means that they incorporate a multitude of atomic lines and molecular bands, which makes abundance information that has been inferred from photometric bands difficult to interpret, and can only be used to infer the collective differences that may be the result of a range of spectroscopic features. In an era where medium to high-resolution spectroscopic data is available, these spectra provide a much more definitive answer to the discussion of subpopulations. We therefore focus on spectroscopic data in this investigation.

In response to the unexpected findings of ML16, two high-resolution spectroscopic studies – both using VLT/FLAMES spectra – have been performed on M4 AGB stars: Mar17 and Wang et al. (2017, W17). Mar17 determined the abundances of a range of species (most relevant to this comparison are the abundances of O, Na, Mg, Al, and Fe) for a sample of 17 AGB stars, but did not re-observe or

redetermine abundances for RGB stars. They reported that their AGB sample showed similar [Na/Fe] and [O/Fe] values to a sample of RGB abundances from [Mar08](#) – on average their AGB sample had [Na/Fe] values only 0.08 dex lower than the RGB sample – thereby challenging the conclusion of [ML16](#) by reporting the discovery of both SP1 and SP2-like AGB stars in M 4.

[W17](#) observed a sample of 19 AGB and 68 RGB stars in M 4, and determined Fe and Na abundances for each star. They reported that their AGB sample shows, on average, lower [Na/H] values than their RGB sample (by 0.14 dex). This was in broad agreement with [ML16](#), however they reported a larger spread in Na abundances on the AGB – $\sigma = 0.17$ dex compared to 0.14 dex in [ML16](#); however their uncertainties in [Na/H] are larger than those determined for our Na abundances (± 0.16 dex compared to ± 0.11 dex). They also noted a smaller difference in maximum [Na/H] between the RGB and AGB ($\Delta[\text{Na}/\text{H}]_{\text{max}} = 0.26$ dex compared to 0.40 dex in [ML16](#)). Curiously, the [Na/H] results of [W17](#) also agreed well with an overlapping sub-sample of [Mar17](#), confusing the situation further since the conclusions of [Mar17](#) and [ML16](#) are in contradiction.

In summary, for our comparison we have collated:

- (i) the O, Na, Mg, Al, and Fe abundances from [I99](#),
- (ii) the CN band strengths from [SB05](#),
- (iii) the O, Na, Mg, Al, and Fe abundances from [Mar17](#) and [Mar08](#),
- (iv) the Na and Fe abundances from [W17](#),
- (v) the O, Na, Mg, Al, and Fe abundances from this study, and
- (vi) CN band strengths from this study.

The evolutionary-phase designation of targets in [I99](#) was questioned in [SB05](#), who reclassified several of the [I99](#) AGB targets. Star 4633 was determined by [SB05](#) and [Suntzeff & Smith \(1991\)](#) to be on the RGB, and here we adopt this classification. Targets 2519, 4201, 1701, and 4414 are listed in [SB05](#) as ‘uncertain’, and we did not include them in our comparison for this reason (we note that their exclusion does not affect the result). For our analysis of the CN band strengths from [SB05](#), we redetermined δS3839 excess values using the green fiducial from [Figure 7](#) to ensure consistency with the CN results of this study.

The studies of [Mar08](#), [Mar17](#), and [W17](#) included many of the same stars in M 4 as [ML16](#), and a direct comparison of the adopted stellar parameters and reported abundances is possible for the overlapping samples. For our comparisons, we use the $\log_e(X)$ notation in order to avoid including systematic offsets such as solar abundance choice and dividing abundances by Fe abundance. Differences between the values determined in this study and those published in [Mar08](#), [Mar17](#), and [W17](#) are summarised in [Table 10](#).

The AGB stellar parameters adopted in this study are largely similar to those in [Mar17](#), while the RGB sample in [Mar08](#) has, on average, higher $\log g$ values by 0.25 dex than our RGB sample, which is likely connected to their Fe I abundances which are systematically larger by 0.09 dex⁷. There are significant offsets between our abundances and those in

[Mar08](#) and [Mar17](#) (up to an average difference of 0.25 dex), however the scatter around these offsets – typically considered a better indication of the agreement between abundance analysis studies – is consistent with the uncertainties quoted in this study. A detailed investigation of the differences in Na abundance between our work and [Mar17](#) (AGB EWs were kindly provided by A. F. Marino via priv. comm.) revealed that all offsets were able to be accounted for by quantifiable differences in stellar parameters, non-LTE corrections, choice of atmospheric models, atomic line data, and EWs. The measured EWs for lines in common (the 568nm doublet) were quite similar, with typical differences of the order of 5 mÅ, corresponding to $\Delta\log_e(\text{Na}) \sim 0.09$ dex.

Comparing our work with that of [W17](#), we note that while the adopted T_{eff} values are quite different (~ 100 K difference), the abundances agree more closely than with [Mar08/Mar17](#). There is still a notable offset in AGB Na abundance ($\Delta\log_e(\text{Na}) = 0.14$ dex), however the large uncertainties quoted in [W17](#) (± 0.16 dex) make it difficult to determine its significance.

We were unable to identify overlapping sample stars with [SB05](#) and [I99](#), and therefore could not directly compare the CN band strengths and elemental abundances from these studies in the same manner.

In order to facilitate comparisons both between the AGB and RGB, and each individual study, we present kernel density estimation (KDE) histograms of the O, Na, Mg, Al, and Fe abundances in [Figures 9, 10, 11, 12, and 13](#), respectively, and KDEs of CN band strengths in [Figure 14](#). The published abundance uncertainties in each study were adopted, and used for the smoothing bandwidths applied to the KDE histograms. We now discuss each element individually.

Iron

The $\log_e(\text{Fe I})$ values as published in [Mar08](#), [Mar17](#), [W17](#), and the Fe abundances determined in this study (§2.4) are presented in [Figure 9](#). In the cases of this study, [W17](#), and [I99](#), the respective samples of RGB and AGB stars were observed simultaneously and analysed in a consistent manner, and the reported Fe abundances agree very well internally, with average differences between the AGB and RGB no larger than 0.04 dex.

In contrast, [Mar17](#) did not observe an RGB sample at the same time as their AGB sample was observed, nor did they re-analyse the results of [Mar08](#) (in which a sample of 105 RGB stars was observed and analysed spectroscopically). Instead, they compared their AGB results directly with their RGB abundances from [Mar08](#). A significant difference in [Fe/H] of 0.14 can be seen between their AGB and RGB samples, larger than the total [Fe/H] uncertainty quoted in either publication. This difference can cause significant problems if elements are scaled by Fe abundance as it implicitly assumes that all other elemental abundances are offset by the same amount. As discussed earlier, we have chosen not to scale abundances with Fe in this study. The reason that the Fe abundances do not agree for these samples is likely to be changes in the adopted spectroscopic method (that, for example, produce systematic offsets in T_{eff} or $\log g$), however we cannot determine the true cause with the available data.

⁷ Ionisation balance was forced in [Mar08](#), which is controlled primarily by $\log g$.

Table 10. The average star-to-star differences in parameters and abundances between the published results of Marino et al. (2017, Mar17, AGB only), Marino et al. (2008, Mar08, RGB only), Wang et al. (2017, W17), and those of this study. Uncertainties are standard deviations, and indicate the scatter between the studies, if the offsets were removed. While significant offsets exist between our work those of Mar17, Mar08 and W17, the scatter around the offsets are consistent with the uncertainties quoted in this study (see text for discussion).

Parameter	Mar17 - this study	Mar08 - this study	W17 - this study	
	(AGB)	(RGB)	(AGB)	(RGB)
ΔT_{eff}	-30 ± 64	-37 ± 61	-94 ± 57	-113 ± 88
$\Delta \log g$	$+0.06 \pm 0.21$	$+0.25 \pm 0.13$	-0.06 ± 0.03	$+0.00 \pm 0.06$
Δv_t	$+0.15 \pm 0.17$	-0.07 ± 0.13	-0.10 ± 0.21	-0.17 ± 0.20
$\Delta \log_{\epsilon}(\text{Fe I})$	-0.02 ± 0.06	$+0.09 \pm 0.07$	$+0.05 \pm 0.09$	$+0.07 \pm 0.11$
$\Delta \log_{\epsilon}(\text{Fe II})$	$+0.03 \pm 0.06$	-	-0.01 ± 0.06	$+0.03 \pm 0.10$
$\Delta \log_{\epsilon}(\text{O})$	-0.10 ± 0.07	-0.03 ± 0.12	-	-
$\Delta \log_{\epsilon}(\text{Na})$	$+0.19 \pm 0.06$	$+0.21 \pm 0.09$	$+0.14 \pm 0.09$	$+0.06 \pm 0.11$
$\Delta \log_{\epsilon}(\text{Mg})$	$+0.10 \pm 0.06$	$+0.22 \pm 0.08$	-	-
$\Delta \log_{\epsilon}(\text{Al})$	$+0.13 \pm 0.04$	$+0.18 \pm 0.08$	-	-

The Fe abundances from neutral lines are very consistent between these studies, except for the disagreement between Mar08 and Mar17. The average abundance for all five studies is $[\text{Fe}/\text{H}] = -1.14 \pm 0.07$ (assuming a solar Fe abundance of 7.50).

Oxygen

The O abundances of this study, Mar17, Mar08, and I99 are presented in Figure 10. Both our re-analysed AGB sample and that of I99 show, on average, slightly higher O abundances than the respective RGB samples ($\Delta \log_{\epsilon}(\text{O}) = 0.08$ for both studies), while the AGB abundances of Mar17 are slightly lower than the RGB values from Mar08 ($\Delta \log_{\epsilon}(\text{O}) = -0.08$). The moderate systematic offsets between studies (up to 0.14 dex) can be largely accounted for by line-list differences (in this study we used the 777nm triplet, while Mar08, Mar17 and I99 used the 630nm forbidden line), however these offsets are still smaller than our uncertainty in $\log_{\epsilon}(\text{O})$.

In our work, the difference between the branches ($\Delta \log_{\epsilon}(\text{O}) = 0.08$) is smaller than the total uncertainty in our O abundances (± 0.15 , see Table 7), and the scatter in our RGB O abundances (± 0.12). We therefore do not make any conclusions about the AGB of M4 from these data. Similarly for the results of Mar17 and I99, the differences between the O abundances of the giant branches are of the order of the uncertainties (± 0.12 and ± 0.08 , respectively), and are therefore too small to claim any significant variation.

These O abundances shed little light on the nature of AGB stars in M4 due to the large uncertainties and relatively small spread in values. Most notable are the O abundances of our work and that of Mar17, whose scatter in $\log_{\epsilon}(\text{O})$ (± 0.12 for Mar17) is of the order of the total reported uncertainty. Furthermore, we detect no bimodality in O abundance, and it is possible that the bimodality seen in the RGB abundances of Mar08 is an artefact of the very small uncertainty of ± 0.04 , which is less than half the magnitude of the O uncertainty in Mar17, which utilised the same method and absorption lines. This casts doubt on the confidence with which a Na-O anti-correlation can be claimed, and it cannot be confirmed that a heterogeneity in O abun-

dance exists within M4 giant stars (Carretta et al. 2009 similarly reported a formal homogeneity in O for M4).

Sodium

The Na abundances reported by Mar17, Mar08, W17, I99, and this study are presented in Figure 11. A significant spread larger than the uncertainties exists within all abundance samples, with many showing strong evidence of bimodality.

In all AGB studies of M4, there is an apparent absence on the AGB of the most Na-rich stars, when compared to the corresponding sample of RGB stars. The various data sets are surprisingly similar, with only one AGB star having $\log_{\epsilon}(\text{Na}) > 5.5$ (in the sample of Mar17); while in all RGB samples, the largest density of $\log_{\epsilon}(\text{Na})$ values is between 5.5 and 5.7. The RGB and AGB of W17 overlap to a larger extent than those of the other studies, but the lack of the most Na-rich stars on the AGB is clear (as noted by W17). The differences between the giant branches in this work, and that of Mar08/Mar17, W17, and I99 are $\Delta \log_{\epsilon}(\text{Na}) = -0.22, -0.21, -0.14,$ and -0.20 , respectively (these values are all larger than the respective uncertainties in Na abundance, except for that of W17).

It is important to note that in all cases there is also evidence of heterogeneity in the Na abundances of M4's AGB population (in this study we found a spread of $\sigma = 0.12$ dex, compared to a total Na uncertainty of ± 0.07 dex). This may indicate that stars that have some Na enrichment (i.e. SP2 stars) are indeed present on the AGB, but that there is a limiting factor that is preventing stars with the highest Na abundances from either evolving to the AGB, or appearing as Na-rich on the AGB as they would have on the RGB. We also note (especially among our abundances, and those of Mar17) that some AGB stars in M4 appear to have lower Na abundances than the most Na-poor RGB stars of the cluster. This suggests that there may be a systematic offset in Na abundance between the two giant branches. We explore this possibility in Section 6.

Finally, we note that the Na abundance uncertainty of W17 (± 0.16 dex) appears to be overestimated, most likely due to the selection of stellar parameters which resulted in an uncertainty in T_{eff} of ± 150 K. The uncertainty in Na

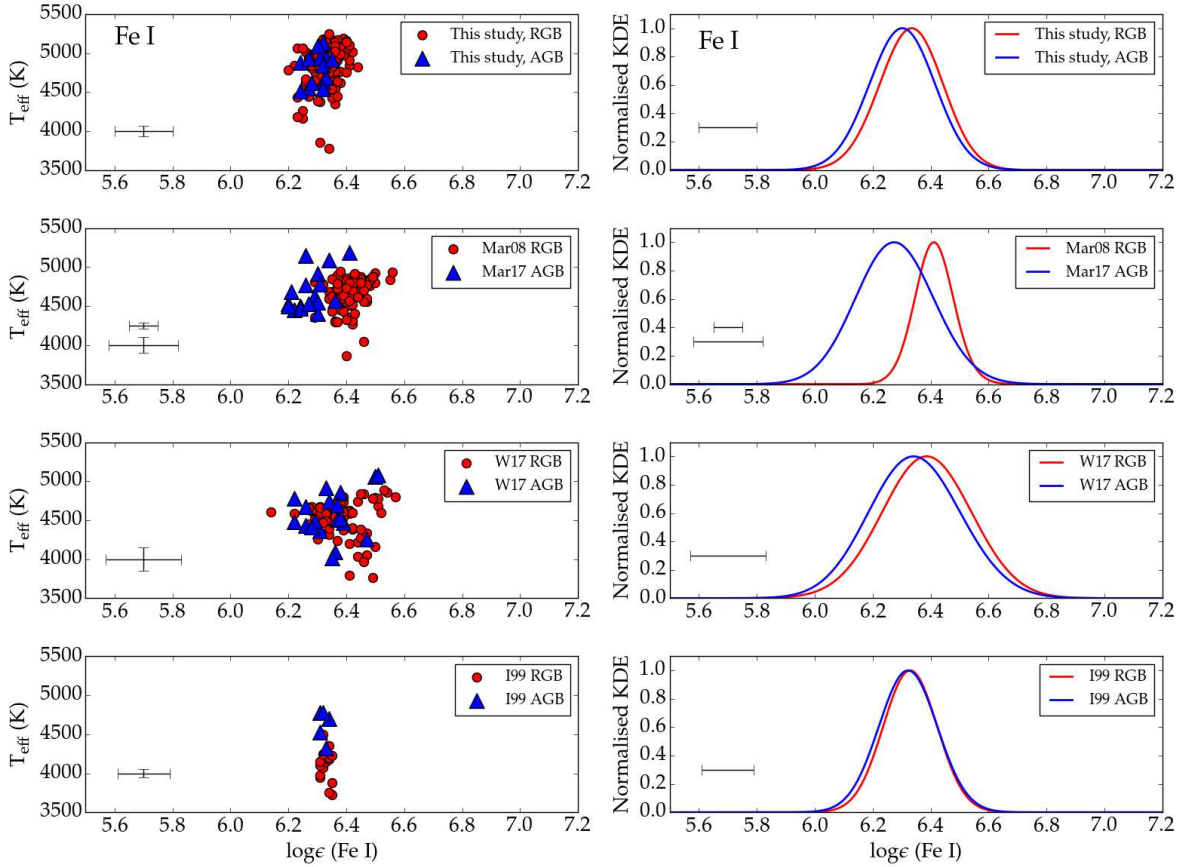


Figure 9. Abundances determined from Fe I absorption lines from this study, Mar17, Mar08, W17, and I99 are presented in the left-hand panels, with kernel density estimations (KDEs) of these data presented in the right-hand panels. Typical abundance errors are shown, as published in the relevant studies (in the Mar17/Mar08 panel the top error bars are those of the RGB sample in Mar08), and were used as the bandwidths of the KDEs in the right-hand panels.

abundance in the study of I99 (± 0.04 dex) appears to be underestimated – the structure seen in the I99 KDE is unlikely to be real, but is more likely an artefact of both small uncertainties and a small sample size – however we chose to adopt the published uncertainties.

Magnesium

Mg abundances from our work, Mar17, Mar08, and I99 are presented in Figure 12. Previous studies have concluded that M 4 is homogeneous in Mg, and we find this for all samples included here.

Due to the homogeneity of Mg, we do not expect any significant difference between the $\log_{\epsilon}(\text{Mg})$ values of AGB and RGB stars in the cluster. While this is the case with the results of this study and those of I99 ($\Delta \log_{\epsilon}(\text{Mg}) = -0.02$ and 0.00, respectively), the abundances of Mar08 and Mar17 indicate that AGB stars in M 4 present as significantly more Mg-poor than the RGB ($\Delta \log_{\epsilon}(\text{Mg}) = -0.14$). We consider this to be unlikely, and it may be related to the discrepancy in Fe abundance between the two studies.

Aluminium

Figure 13 presents the Al abundances of this study, Mar17, Mar08, and I99. The spread in RGB $\log_{\epsilon}(\text{Al})$ values, while significant in each sample at the 1σ level (± 0.09 , ± 0.12 , and ± 0.12 for our work, Mar08, and I99, respectively) is quite small and there is no evidence of bimodality. The spread in AGB Al abundances, however, is even smaller than for each of the respective RGB samples, and shows potentially homogeneous abundances (except for the single Al-rich outlier in this study and Mar17; 2MASS ID 16234085-2631215).

The similarity between the Al abundances of this study, Mar17, and I99 is noteworthy, with the AGB samples in all cases being significantly offset to lower values ($\Delta \log_{\epsilon}(\text{Al}) = -0.14$, -0.18 , and -0.18 , respectively), indicating that M 4 stars on the AGB are more Al-poor, on average, than those on the RGB.

While the Al abundance uncertainty reported in I99 (± 0.03 dex) appears to be underestimated (as with Na), we adopt this value for our comparison while noting that the structure in the bottom right panel of Figure 13 is likely an artefact of this underestimation.

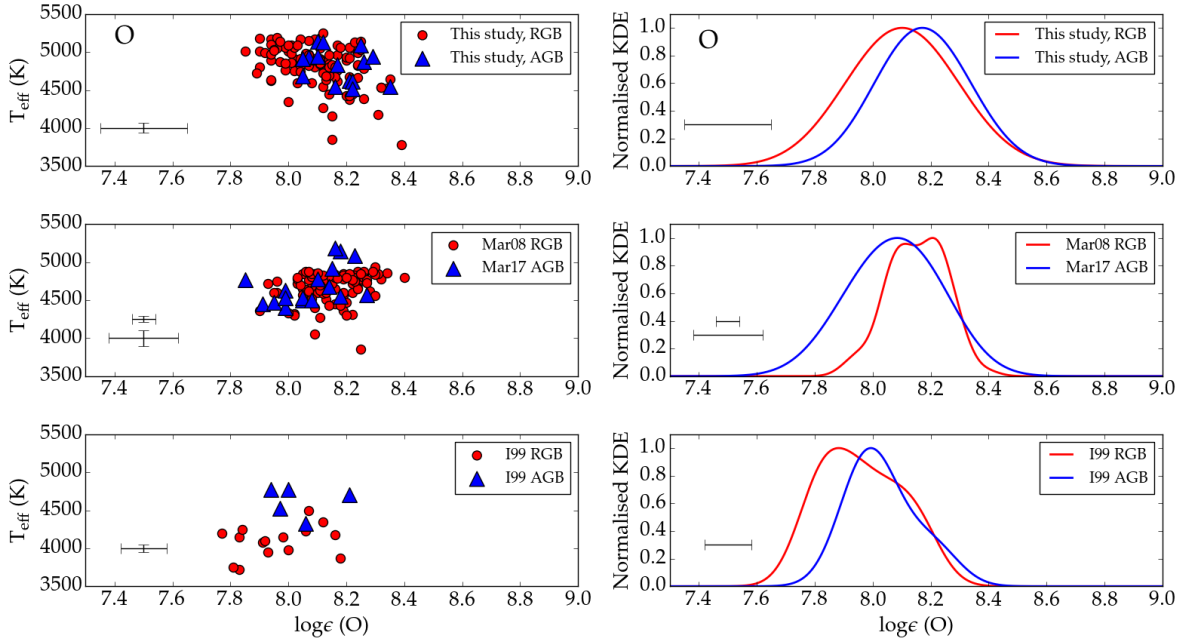


Figure 10. Same as Figure 9, but for the abundances determined from O I absorption lines from this study, Mar17, Mar08, and I99.

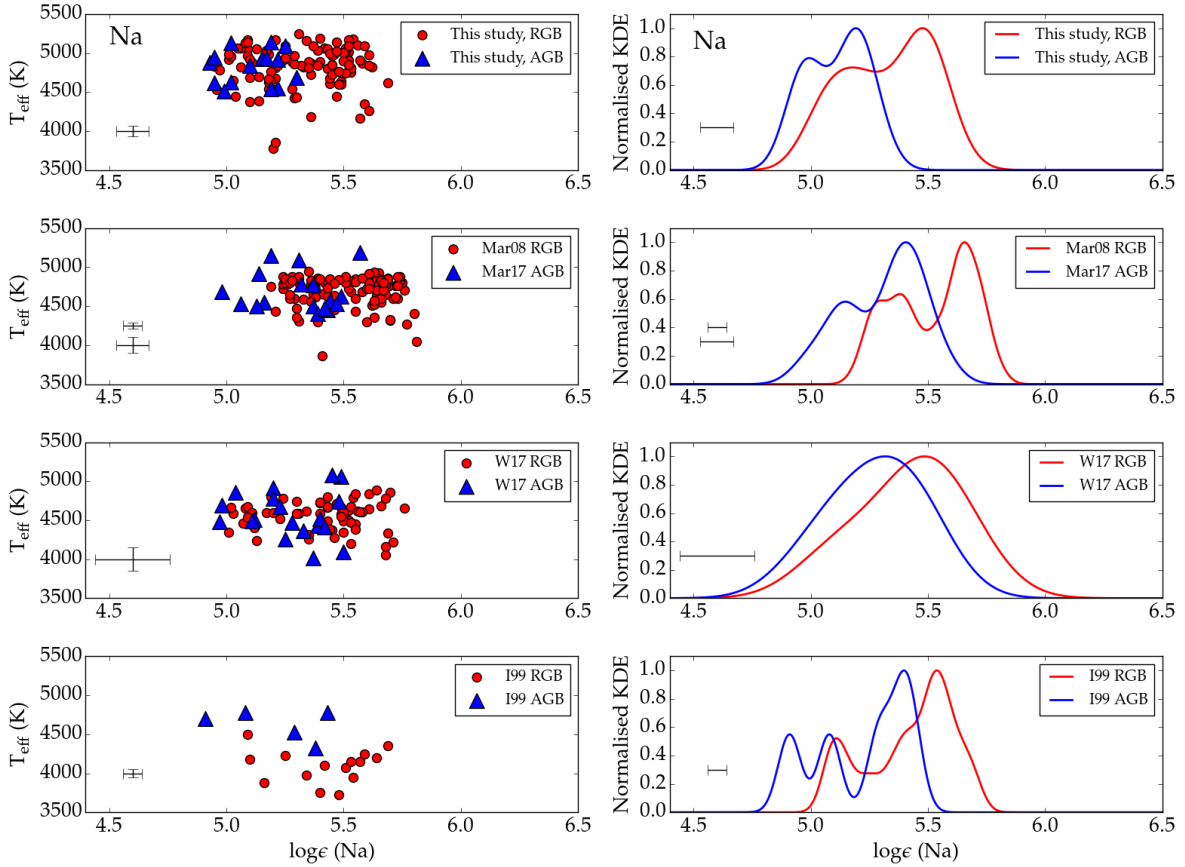


Figure 11. Same as Figure 9, but for the abundances determined from Na I absorption lines from this study, Mar17, Mar08, W17, and I99.

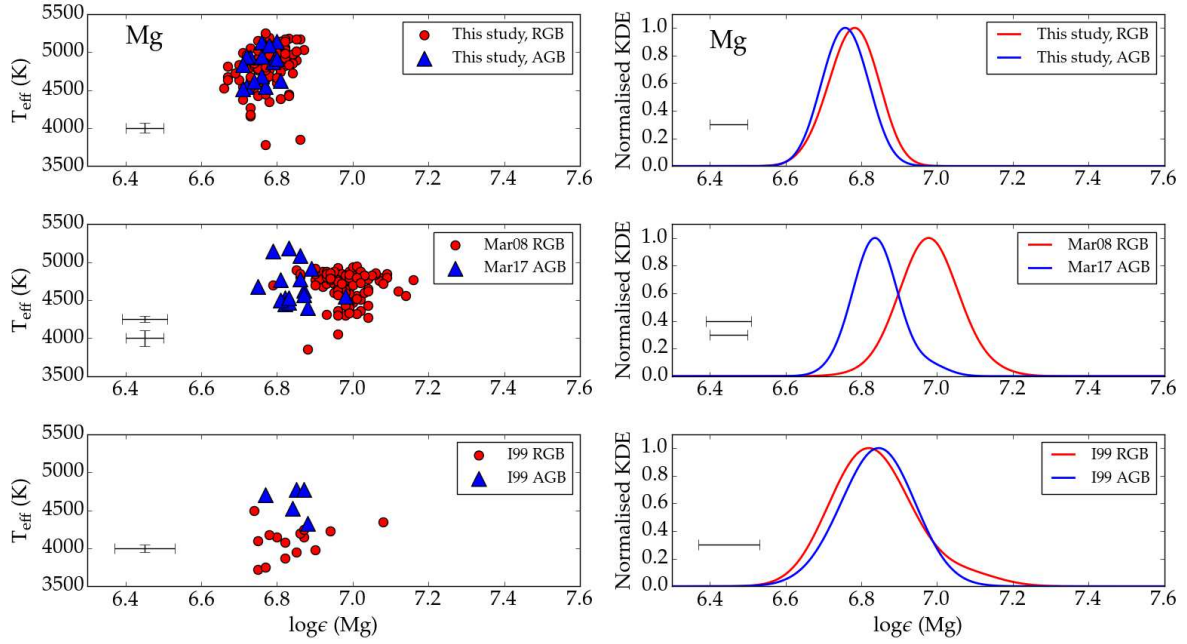


Figure 12. Same as Figure 9, but for the abundances determined from Mg I absorption lines from this study, Mar17, Mar08, and I99.

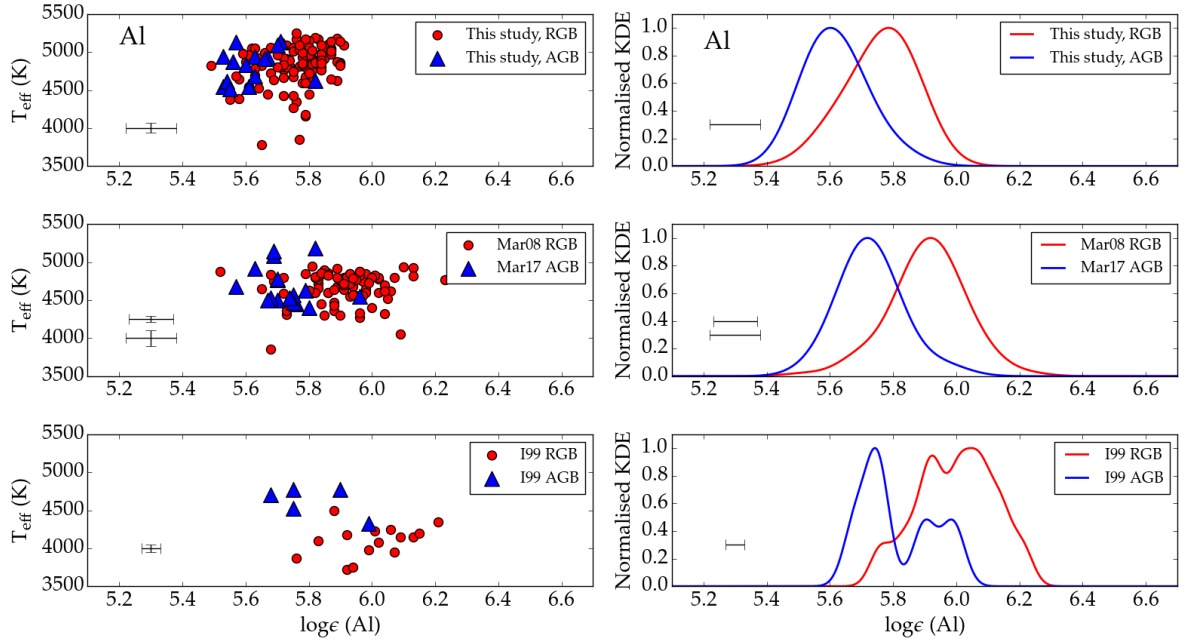


Figure 13. Same as Figure 9, but for the abundances determined from Al I absorption lines from this study, Mar17, Mar08, and I99.

Cyanogen

In Figure 14, the compiled CN band strengths of SB05 and the results from this study (from §3) are presented. A clear bimodality in $\delta S3839$ values is visible in the RGB samples of both studies (albeit with a larger spread of ± 0.25 in the results from this study, compared to ± 0.19 in SB05), which has been noted in previous CN studies of M 4 (Norris 1981; Suntzeff & Smith 1991).

Both studies strongly suggest an extreme paucity of CN-strong AGB stars in the cluster: $\Delta\delta S3839 = -0.20$ and -0.14 for this study and SB05, respectively. In both AGB samples, however, there is a significant spread in $\delta S3839$ values (± 0.12 and 0.11 , respectively), with an apparent bimodality in the AGB sample of SB05 (although there are only 6 stars in this sample). This striking similarity between the independently observed and analysed CN results pro-

vides significant weight to our Na and Al abundance results, along with the strong correlation between $\delta S3839$ and $\log_\epsilon(\text{Na})$ values (see Figure 8).

Comparison Summary

In summary, we have identified four main conclusions from the literature comparison:

- (i) there is no systematic offset between the Mg and Fe abundances of AGB and RGB stars in M4,
- (ii) the AGB of M4 is systematically offset to lower values in Na and Al abundances, and CN band strength compared to the RGB,
- (iii) no conclusions can be drawn concerning differences in the O abundances of AGB or RGB stars in M4, and
- (iv) due to (iii) there may be no Na-O anti-correlation in M4.

Three of the most common diagnostic tools of multiple populations in M4 – Na abundances, Al abundances, and CN band strengths – consistently indicate a significant difference between the light-elemental distributions of AGB and RGB stars in this globular cluster, with an apparent deficit of AGB stars enhanced in H-burning products. The only exception to this are the O abundances, from which no conclusion can be consistently drawn. Indeed, we detect little evidence of a spread in O abundance for M4. Thus, taken at face value, most of the results presented in this section show that, in general, the AGB stars in M4 contain less H-burning products than RGB stars in the cluster. It is possible that the stars currently on the AGB have experienced less of the ‘self-pollution’ that M4 (and other Galactic GCs) is thought to have experienced early in its life (D’Orazi & Marino 2010).

We can see only two possible explanations for the results presented here:

- (i) The most Na-enhanced – and by correlation, He-enriched (D’Antona et al. 2002; Chantereau et al. 2016) – stars in M4 are not evolving to the AGB, but are becoming AGB-manqué stars, evolving directly from the HB to the WD phase.
- (ii) Systematic errors are affecting both the high-resolution spectroscopic method of abundance determination *and* the calculation of S3839 index values of AGB stars across several studies, consistently resulting in AGB samples appearing more Na-poor, Al-poor, and CN-weak than they are in reality.

We investigate i) in §5 with 1D stellar evolution models, and ii) in §6 by conducting tests on the impact of using a range of different atmospheric models for the determination of elemental abundances.

5 EXPECTATIONS FROM THEORETICAL STELLAR EVOLUTION MODELS

In the stellar evolutionary models of Dorman et al. (1993), at the approximate metallicity of M4 ($[\text{Fe}/\text{H}] \sim -1.15$), stars with zero-age HB (ZAHB) effective temperatures of $15,000 \lesssim T_{\text{eff}} \lesssim 19,000$ K have short early-AGB lives and

evolve to the white dwarf cooling phase without fully ascending the AGB. These stars may not be detectable on the AGB due to the short time-scale of this phase of evolution. Stars with $T_{\text{eff}} \gtrsim 19,000$ K at the ZAHB become AGB-manqué stars and never join the AGB. If applied to M4, this implies that *all* stars in M4 should evolve to and ascend the AGB. This is because the hottest HB stars in the cluster have $T_{\text{eff}} \sim 9500$ K (Villanova et al. 2012).

The spectroscopic abundances of M4’s AGB population, as presented in this study, appear to suggest that the most Na-rich stars (these stars populate the blue-HB due to the correlation between He and Na abundance; Marino et al. 2011; Chantereau et al. 2016) either do not evolve to the early-AGB, or spend a very short amount of time in this phase⁸.

To establish a precise, quantitative theoretical expectation of M4’s AGB abundances we have calculated a range of theoretical stellar model tracks for M4 stars. We have done this in order to determine the likelihood of the blue HB stars in the cluster avoiding the AGB, thereby intrinsically creating the abundance distributions observed in this study – where the most Na-rich stars are present on the HB, but missing on the AGB. The stellar models were calculated using the Monash University stellar structure code MONSTAR (Lattanzio 1986; Campbell & Lattanzio 2008) with Spruit (2015) overshooting in the core helium-burning phase, as described in Constantino et al. (2017). The code has been updated with low temperature opacity tables which follow variations in C, N and O (Marigo & Aringer 2009; Constantino et al. 2014). The Reimers (1975) mass loss prescription was used for the RGB.

Our aim was to determine the optimal parameters for M4 stars that allowed us to most accurately match the observed bimodal HB, and to identify whether these stars evolve to the AGB. We then sought to determine the approximate HB T_{eff} required for M4 stars to avoid the AGB phase. At a given age and metallicity, the HB T_{eff} of a star is a function of both initial mass⁹ and helium mass fraction – a higher Y value decreases the time on the main sequence, so for a coeval cluster with a helium abundance variation, a star enhanced in He will have a lower initial mass, and therefore have a higher HB T_{eff} .

We began by identifying the most important observational and theoretical constraints that affect HB morphology, and created a range of parameters over which to test. We tested three parameters: helium enrichment (ΔY), cluster age, and RGB mass loss rate. Cluster metallicity also has an effect on HB morphology, however, this value is well constrained for M4 – therefore we assumed $[\text{Fe}/\text{H}] = -1.15$ for all evolutionary models. Published estimates of these constraints from the literature, and the values adopted for our evolutionary models, are summarised in Table 11.

For the helium mass-fraction of SP1 stars in M4 we adopted $Y = 0.245$ (Valcarce et al. 2014), and for SP2 stars we adopted $Y = 0.275$ (so $\Delta Y = 0.03$, see Table 11). For

⁸ Such that no such Na-rich stars are in the AGB phase at the present time.

⁹ Since the core mass at the onset of helium burning is relatively fixed at $\sim 0.475 M_\odot$ due to the degenerate equation of state (Sweigart & Gross 1978), the amount of leftover envelope after the core helium flash directly influences the HB T_{eff} .

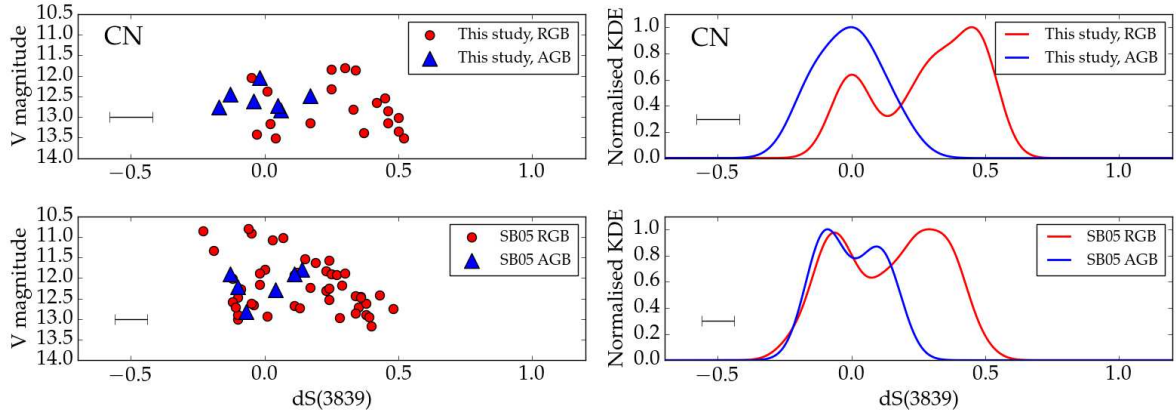


Figure 14. Same as Figure 9, but for the CN band strengths (δS_{3839} values) from this study and SB05.

Table 11. A summary of M 4 observational constraints for helium enrichment (ΔY), age, and RGB mass loss parameter (Reimers η). The values adopted for use in our theoretical models are listed in the last row.

Reference	ΔY	Age (Gyr)	Reimers η
H02 ¹	-	12.70 ± 0.70	-
MF09 ²	-	12.65 ± 0.64	-
V12 ³	0.04	-	-
Val14 ⁴	$\lesssim 0.01$	-	-
MZ15 ⁵	-	11.81 ± 0.66	0.40 ± 0.08
N15 ⁶	0.02	-	-
Adopted	0.03	12.45 ± 0.7	0.40 ± 0.08

¹Hansen et al. (2002); ²Marín-Franch et al. (2009)

³Villanova et al. (2012); ⁴Valcarce et al. (2014)

⁵McDonald & Zijlstra (2015); ⁶Nardiello et al. (2015)

C, N and O abundances, we adopted the values reported by Villanova et al. (2012) for the N-poor (SP1) and N-rich (SP2) populations¹⁰. We calculated models over a range of ages (determined primarily by initial mass and Y , for which the dependence was controlled) and RGB mass loss rates. We compared the maximum T_{eff} reached on the HB – our primary observational constraint – with observed values reported in the literature, as determined by Marino et al. (2011, maximum red-HB $T_{\text{eff}} = 6250$ K) and Villanova et al. (2012, maximum blue-HB $T_{\text{eff}} = 9500$ K). A summary of our model tracks is presented in Table 12.

We found that in order to match the HB morphology of M 4, based on spectroscopic HB T_{eff} values and helium mass-fractions in the literature, we required a Reimers mass loss rate of $\eta = 0.44 \pm 0.04$ and initial masses of 0.827 ± 0.013 and $0.785 \pm 0.013 M_{\odot}$ for SP1 and SP2, respectively; which gave a cluster age of 12.4 ± 0.6 Gyr. Uncertainties given here are the ranges in each value for which the HB morphology was able to be reproduced.

In Figure 15 we present model tracks with the mean

mass loss rates and initial masses required to match the HB of M 4 (according to the maximum T_{eff} reached on the HB), which are indicated in bold text in Table 12. Included for reference are the stellar parameters (reported T_{eff} and photometric $\log g$) of HB stars determined by Marino et al. (2011) and Villanova et al. (2012), and AGB stars determined with PHOBOS v2 in this study. As an example of an AGB-manqué star, we also included a stellar model with a very large helium enhancement ($Y = 0.32$ and $\Delta Y = 0.08$, see Table 12), for which we adopted the mean age and mass loss rate that we determined for M 4 (12.4 Gyr, $\eta = 0.44$).

All stellar models whose maximum T_{eff} on the HB closely matched the values in the literature (6250 K for the red-HB, and 9500 K for the blue-HB) evolved to the AGB. In fact, all models with a maximum HB $T_{\text{eff}} \lesssim 15,500$ K spend enough time on the early-AGB to potentially be observed. This provides a very strong prediction that every star in M 4 should evolve to (at least) the early-AGB, and that the light elemental abundance distribution of the AGB should match that of the HB and RGB. Furthermore, we find that only HB stars with a maximum $T_{\text{eff}} \gtrsim 15,500$ K are likely to avoid the AGB, or have short enough AGB-lifetimes to avoid detection – this agrees well with the HB models of Dorman et al. (1993). We note that there is a difference of 6000 K in T_{eff} between the observed blue end of M 4’s HB and the values required for the evolution of AGB-manqué stars. Comparing to the reported uncertainty in T_{eff} of ± 50 K in Marino et al. (2011) and Villanova et al. (2012), this is a very large difference. This shows that there is a very clear expectation that *all* stars on the M 4 blue-HB should become AGB stars.

In chemical space, this implies that the Na, Al, and CN distributions should be identical on the AGB and RGB. Given the abundance results from multiple spectroscopic studies (see §4), which indicate that these abundance distributions are *not* identical, there is a clear discordance between the observations of M 4 stars and theoretical expectations.

In the next section, we investigate various uncertainties and assumptions that may affect the abundances of AGB stars in M 4, to see whether aspects of the spectroscopic method may be responsible for the contradictory results found thus far.

¹⁰ SP1: $[C/Fe] = -0.20$, $[N/Fe] = +0.16$, $[O/Fe] = +0.42$.

SP2: $[C/Fe] = -0.36$, $[N/Fe] = +0.80$, $[O/Fe] = +0.25$.

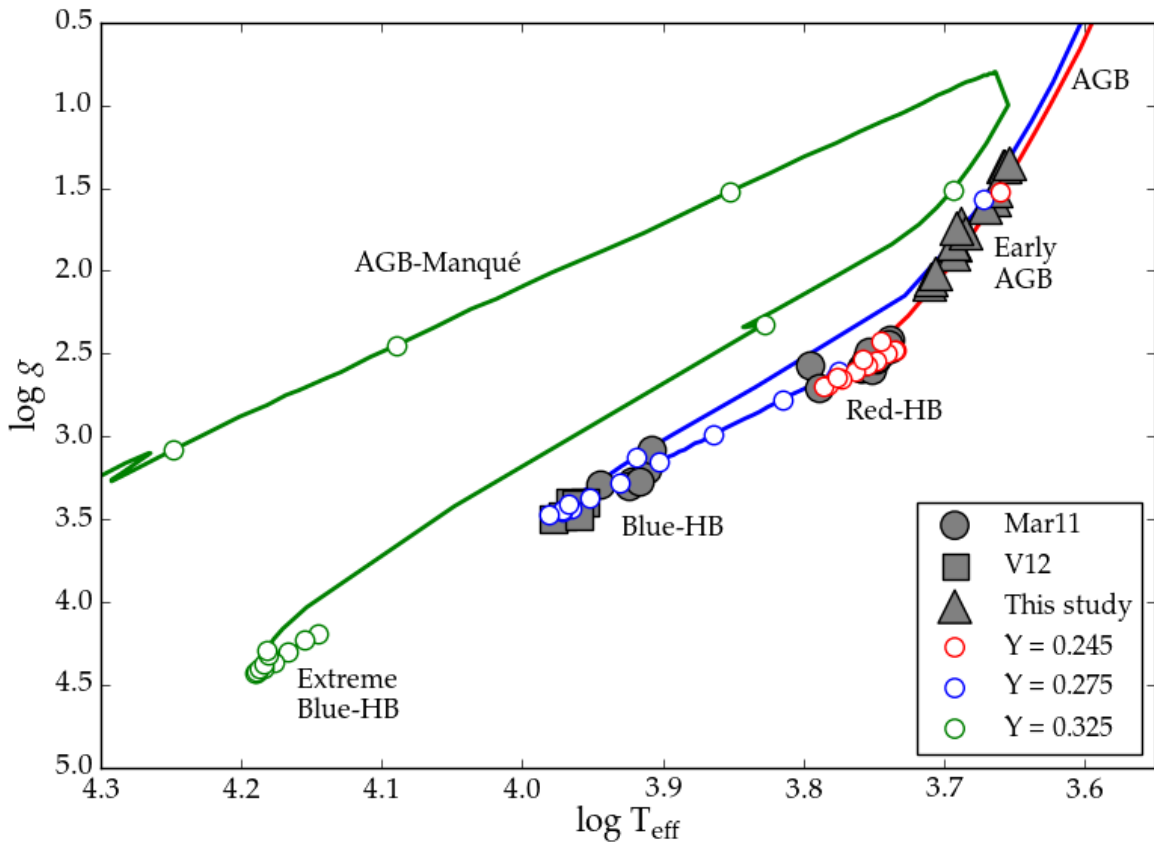


Figure 15. Evolutionary tracks of the three models found to best match the red-HB (red track, $Y = 0.245$), the blue-HB (blue track, $Y = 0.275$), and the lowest HB T_{eff} required to produce an AGB-manqué star (green track, $Y = 0.325$) – see Table 12 and text for model details. While each model was evolved from the beginning of the main sequence, we show the evolution of each model from the ZAHB. Points along the evolutionary tracks are separated in age by 10 Myr to give an indication of time spent in each phase, and hence the likelihood of observing stars in each phase. Also included are the T_{eff} and $\log g$ values for our AGB sample (from §2), and the T_{eff} values of HB stars from Marino et al. (2011, Mar11) and Villanova et al. (2012, V12) for which we redetermined $\log g$ photometrically (using the empirical relation from Alonso et al. 1999, so that all observations are on the same $\log g$ scale). Also note that the blue-HB model begins on the red-HB before quickly moving to canonical blue-HB temperatures, possibly indicating that some red-HB stars may in fact be SP2 stars that are still in the early HB phase. While Marino et al. (2011) did not report on any Na-rich stars on the red-HB, they did find a larger spread of Na abundances among red-HB stars than blue-HB stars.

6 ATMOSPHERIC MODEL TESTS

6.1 Stellar parameter test

Determining precise effective temperatures for stars can be difficult – random and systematic errors are often of the order of 100 – 200 K (e.g. Ramírez & Meléndez 2005; Wang et al. 2017, also see Table 2, Figure 2, and Table 10). While the random errors in our work that are associated with uncertainties in atmospheric parameters are presented in Table 6, we conducted an additional test of stellar parameters, in an effort to investigate the effects of systematic errors in T_{eff} on our sample of M4 stars.

We redetermined LTE Na and Fe abundances for our M4 stellar sample using three different empirical colour- T_{eff} relations (see §2.2), chosen to maximise the systematic differences between the estimated effective temperatures. These relations are the $B - V$ relation from Alonso et al. (1999), the $B - V$ relation from Casagrande et al. (2010), and the $V - K$ relation from Ramírez & Meléndez (2005,

note that some stars do not have reliable 2MASS magnitudes and were therefore not included here). The average differences between the T_{eff} values determined from these relations and those adopted for our final $T_{\text{eff,sp}}$ results in §2 are 1 ± 67 K, -83 ± 105 K and 129 ± 109 K, respectively. The star-to-star differences are presented in Figure 16, showing individual T_{eff} differences of up to 500K and a total 1σ scatter of 127 K for the entire sample. Values of $\log g$ and v_t were determined using the same method as in §2.2.

The LTE Fe and Na abundances determined using the stellar parameters from these three relations (the line-list and method are the same as in §2) are presented in Figures 17 and 18. Systematic differences in T_{eff} have a large effect on the spread and distribution of Fe abundances, with the Casagrande et al. (2010) and Ramírez & Meléndez (2005) relations producing significant trends between T_{eff} and $\log_{\epsilon}(\text{FeI})$ (also see C17). Our adopted $T_{\text{eff,sp}}$ values (included in the bottom panels for comparison) produce the tightest distribution of Fe abundances ($\sigma = 0.05$).

Table 12. A summary of theoretical stellar models calculated for M4. The last column indicates the highest T_{eff} that was reached in the HB phase of each model track, our primary observational constraint. The first ten models listed are representative of SP1 stars, with a T_{eff} constraint on the red-HB from [Marino et al. \(2011\)](#). The next ten models are representative of SP2 stars, with a T_{eff} constraint on the blue-HB from [Villanova et al. \(2012\)](#). The final nine models are tests using extreme values of RGB mass loss, age, and helium enrichment, to explore AGB-manqué evolution. In Figure 15 we show tracks of the three models in bold text, which we found to best match the red-HB ($Y = 0.245$), the blue-HB ($Y = 0.275$), and also the lowest HB T_{eff} required to produce an AGB-manqué star ($Y = 0.325$).

Y	Age (RGB-tip) (Gyr)	Initial Mass (M_{\odot})	Reimers η	HB Max T_{eff} (K)
<i>SP1 (Observed HB Max $T_{\text{eff}} = 6250$ K)</i>				
0.245	11.83	0.839	0.32	5375
0.245	11.83	0.839	0.40	5540
0.245	11.83	0.839	0.47	6030
0.245	12.45	0.827	0.32	5425
0.245	12.45	0.827	0.40	5675
0.245	12.45	0.827	0.44	6120
0.245	12.45	0.827	0.47	6960
0.245	13.24	0.813	0.32	5510
0.245	13.24	0.813	0.40	6050
0.245	13.24	0.813	0.47	8250
<i>SP2 (Observed HB Max $T_{\text{eff}} = 9500$ K)</i>				
0.275	11.79	0.796	0.32	5720
0.275	11.79	0.796	0.40	7250
0.275	11.79	0.796	0.47	9370
0.275	12.40	0.785	0.32	6025
0.275	12.40	0.785	0.40	8150
0.275	12.40	0.785	0.44	9400
0.275	12.40	0.785	0.47	10390
0.275	13.22	0.771	0.32	6950
0.275	13.22	0.771	0.40	9380
0.275	13.22	0.771	0.47	11870
<i>Tests of extreme η values</i>				
0.275	12.40	0.785	0.55	13530
0.275	12.40	0.785	0.58	15200
0.275	12.40	0.785	0.60	17000
<i>Tests of extreme ages</i>				
0.275	14.59	0.750	0.44	13070
0.275	15.70	0.735	0.44	16000
<i>Tests of extreme Y values</i>				
0.295	12.40	0.757	0.44	11840
0.315	12.40	0.729	0.44	14500
0.325	12.40	0.715	0.44	15500
0.350	12.40	0.680	0.44	19200

In contrast to the effect on Fe abundance, large systematic variations in T_{eff} appear to have little impact on the distribution of Na abundances, despite some stars' T_{eff} varying by up to nearly 500 K between the three empirical relations and those adopted in this study. As seen in Figure 18, the Na-poor nature of our AGB sample is present irrespective of the T_{eff} scale adopted. This demonstrates that conservative systematic changes in stellar atmospheric parameters have virtually no bearing on our results, and that $\log_{\epsilon}(\text{Na})$ is much more robust to sample-wide T_{eff} variations than $\log_{\epsilon}(\text{Fe I})$ (which we also found to be the case for NGC 6752;

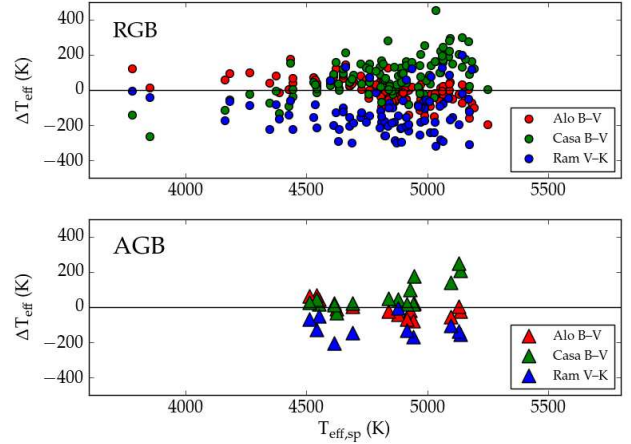


Figure 16. The star-to-star differences in T_{eff} between our $T_{\text{eff,sp}}$ values and those of three empirical colour- T_{eff} relations: [Alonso et al. \(1999, \$B - V\$ \)](#), [Casagrande et al. \(2010, \$B - V\$ \)](#), and [Ramírez & Meléndez \(2005, \$V - K\$ \)](#), where $\Delta T_{\text{eff}} = T_{\text{eff,relation}} - T_{\text{eff,sp}}$. The top panel shows our sample of RGB stars in M4, while the bottom panel presents our AGB sample.

see [C17](#)). Next, we investigated the effect of including helium enhancement in atmospheric models.

6.2 Helium enriched model test

The KURUCZ/ATLAS9 atmospheric models used in the determination of abundances in this study adopt the solar abundances of [Grevesse & Sauval \(1998\)](#) – with a helium mass fraction of $Y = 0.248$, which is similar to the primordial value assumed for SP1 stars in M4 ($Y \sim 0.245$; [Valcarlos et al. 2014](#)). It is accepted that some GC stars are significantly enriched in helium (by more than $\Delta Y = 0.15$ in some clusters, for example NGC2808; [D’Antona et al. 2005](#)). [Villanova et al. \(2012\)](#) determined helium abundances for a sample of blue HB stars in M4 (assumed to represent the most He-rich stars in the cluster), and found ΔY to be of the order of 0.03-0.04, while [Valcarlos et al. \(2014\)](#) and [Nardiello et al. \(2015\)](#) determined ΔY values of $\lesssim 0.01$ and 0.02, respectively.

Here we investigate the effects of including a He-enhancement in the atmospheric models used in chemical abundance determination. We redetermined the LTE abundances of O, Na, Mg, Al, and Fe for a sub-sample of M4 stars using a representative helium rich model available in the ATLAS9 database. Few He enhanced models have been computed for the ATLAS9 grid, so we conducted this test using the model with parameters closest to our M4 sample: $[\text{Fe}/\text{H}] = -1.5$, $T_{\text{eff}} = 5000$ K, $\log g = 1.5$, $v_t = 2.0$ km/s, and $\Delta Y = +0.1$ ($Y = 0.352$). Due to the restriction of model selection, only a small subset of stars in our sample have stellar parameters similar to this model; therefore only a representative test was possible.

For a sub-sample of four AGB and eight RGB stars (which cover the entire range of Na abundance as determined with PHOBOS v2), we determined LTE abundances using: i) the He enhanced model (‘Y-enh/ α -norm’) which has scaled solar abundances for all other species, ii) a model

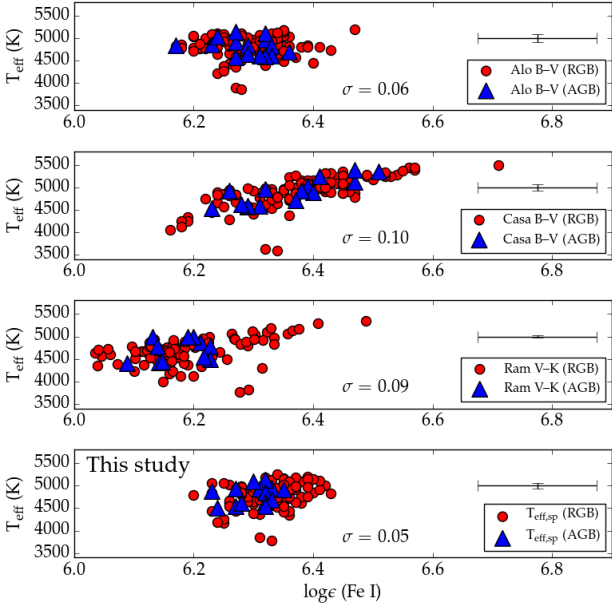


Figure 17. Fe abundances plotted against T_{eff} , as determined using three different empirical colour- T_{eff} relations (top three panels) – Alonso et al. (1999, $B-V$), Casagrande et al. (2010, $B-V$), and Ramírez & Meléndez (2005, $V-K$) – and our spectroscopic stellar parameters ($T_{\text{eff,sp}}$, using PHOBOS; bottom panel). The total uncertainty in $\log_{\epsilon}(\text{Fe I})$ is indicated (see Table 7), along with the relevant quoted uncertainties in T_{eff} for each relation.

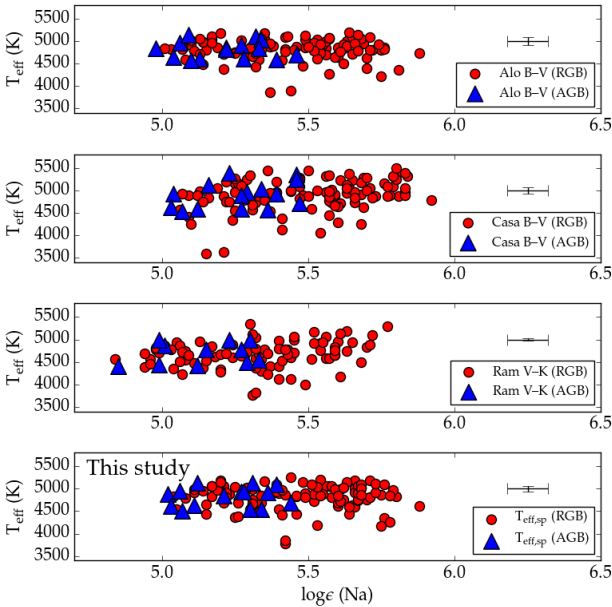


Figure 18. Same as Figure 17, but for Na abundance.

with scaled solar abundances and $Y = 0.248$ (‘Y-norm/ α -norm’), and iii) a model with $Y = 0.248$ and an α -element enhancement of $+0.4$ dex (‘Y-norm/ α -enh’). With these three models¹¹, we were able to quantify the effect of increased He on elemental abundances while controlling for α -enhancement (α -enhanced atmospheric models were adopted for our abundance determination in §2.3). All three models had the same values of $[\text{Fe}/\text{H}]$, T_{eff} , $\log g$, and v_t to ensure a consistent comparison. The results of this test are summarised in Table 13.

The differences between the abundances determined using the two $Y = 0.248$ models (‘Y-norm/ α -enh’ and ‘Y-norm/ α -norm’; see column three of Table 13), were constant throughout the sub-sample of 12 stars. Therefore we found that the effects of an α -enhancement are small and entirely systematic, with offsets ≤ 0.04 dex for all species.

Similarly, the effects of helium enhancement were systematic – that is, an offset across the test sample – for every species except Na, for which there was a 0.04 dex ($\sigma = 0.01$) range in abundance differences. This was smaller than our total uncertainty in $\log_{\epsilon}(\text{Na})$ of 0.07 dex. As seen in Figure 19, which presents the quantitative effect of He-enhancement on Na abundance for the 12 stars in our sub-sample, the relative increase in Na abundance when the ‘Y-enh/ α -norm’ model is used positively correlates with Na abundance. Notably, the maximum change in Na abundance (0.08 dex) is of the order of our uncertainties (± 0.07 dex), and is significantly smaller than the mean difference in abundance between the RGB and AGB ($\Delta \log_{\epsilon}(\text{Na}) = 0.22$ dex in our work).

We conclude that using helium enhanced 1D atmospheric models for the determination of chemical abundances of helium enriched stars in M4 would not alter the findings of this study for the following reasons:

(i) The ‘Y-enh/ α -norm’ model affects the Na abundance of AGB stars in the same direction and magnitude as RGB stars of similar parameters and Na abundance, so distributions are not altered.

(ii) A helium enhancement of $\Delta Y = +0.1$ dex alters $\log_{\epsilon}(\text{Na})$ by $\lesssim 0.07$ dex, which is smaller than our uncertainty in $\log_{\epsilon}(\text{Na})$. Therefore, a helium enhancement more appropriate to M4 ($0.01 < \Delta Y < 0.04$) would most likely not produce a measurable change in Na abundance.

(iii) A helium enhancement preferentially spreads out the high-Na stars to even higher values, making the AGB stars even more representative of SP1 RGB stars.

6.3 MARCS and (3D) STAGGER-grid test

In this study, and our previous GC investigations using AAT/HERMES spectra (ML16 and ML18a), we have exclusively employed the ATLAS9 grid of stellar atmospheric models. As a further test of the effects of using different model atmospheres on abundance determination, we investigate the effect on chemical abundance when two other sets of atmospheric models are employed: the 1D MARCS grid, and the mean-3D STAGGER-grid. Moreover, we do this with

¹¹ There are no ‘Y-enh/ α -enh’ models in the ATLAS9 database.

Table 13. The average differences in elemental abundance, for a representative sub-sample of M 4 stars, when three ATLAS9 atmospheric models of varying composition – helium-enhanced/ α -normal ('Y-enh/ α -norm'), helium-normal/ α -normal ('Y-norm/ α -norm'), and helium-normal/ α -enhanced ('Y-norm/ α -enh') – were used, in combination with our standard spectroscopic method of abundance determination. All three models had the following stellar parameters: $[\text{Fe}/\text{H}] = -1.5$, $T_{\text{eff}} = 5000$ K, $\log g = 1.5$, $v_t = 2.0$ km/s, while the T_{eff} of each star in our sub-sample (8 RGB, and 4 AGB stars) was between $4900 < T_{\text{eff}} < 5100$ K. Errors are the standard deviation of abundance difference over our 12 star sub-sample.

Species	$\Delta \log_{\epsilon}(\text{X})$	
	(Y-enh/ α -norm – Y-norm/ α -enh)	(Y-norm/ α -enh – Y-norm/ α -norm)
Fe I	$+0.029 \pm 0.003$	-0.023 ± 0.001
Fe II	-0.013 ± 0.004	$+0.040 \pm 0.001$
O	$+0.092 \pm 0.002$	$+0.010 \pm 0.006$
Na	$+0.050 \pm 0.012$	-0.020 ± 0.002
Mg	$+0.041 \pm 0.002$	-0.017 ± 0.001
Al	$+0.024 \pm 0.002$	-0.011 ± 0.000

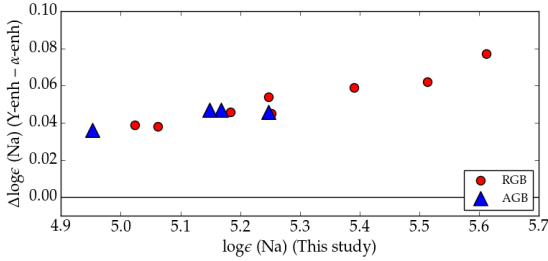


Figure 19. The star-to-star differences in Na abundance, for a representative sub-sample of 12 M 4 stars, when two ATLAS9 atmospheric models of varying composition – helium-enhanced and α -enhanced – were used, in combination with our standard spectroscopic method of abundance determination. Na abundances on the x-axis are those adopted as the final abundances in this study.

a totally independent abundance determination code, providing a further test of the robustness of our results.

We determined non-LTE $\log_{\epsilon}(\text{Na})$ and $\log_{\epsilon}(\text{O})$ values for our entire M 4 sample using the 3D non-LTE BALDER code (Amarsi et al. 2018a; based on the MULTI3D code, Leenaarts & Carlsson 2009). This method was very different to that used in Section 2.3. Synthetic equivalent widths were calculated across a grid of Na and O abundances (in steps of 0.2 dex) by direct integration across the line, and then interpolated onto our spectroscopic stellar parameters (determined with PHOBOS v2). Abundances were evaluated by interpolating $[\text{X}/\text{Fe}]$ values (a constant value of $[\text{Fe}/\text{H}] = -1.17$ was adopted) as a function of synthetic equivalent width onto our measured equivalent widths (from §2.3) for each star. Calculations were based on the Na model atom from Lind et al. (2011), and the O model atom from Amarsi et al. (2018b).

This abundance determination was done twice for our entire M 4 stellar sample, with different grids of atmospheric models: i) the spherical 1D MARCS model atmospheres of scaled-solar chemical composition and $v_t = 2.0$ km/s (Gustafsson et al. 2008), and ii) the spatially- and temporally-averaged mean 3D ($\langle 3D \rangle$) model atmospheres of the STAGGER-grid (Magic et al. 2013). For the latter analysis (based on $\langle 3D \rangle$ model atmospheres), several stars in our sample, including all AGB stars, required extrapolation in

T_{eff} or $\log g$, as they lie outside the parameter space of the STAGGER-grid.

Abundances determined using the BALDER code in combination with the MARCS grid are presented in Figure 20, along with the star-to-star differences in non-LTE Na abundances between those from Section 2.4 and those from this test. The results of this test are also presented in Table 14. Comparing the top panel in Figure 20 with Figure 5 shows that the spread and distribution of O and Na abundances using the MARCS grid and the BALDER code are similar to those determined with PHOBOS v2. The bottom panel, however, indicates that significant changes to the absolute Na abundances occurred. The differences between the models and methods are correlated with Na abundance, and not evolutionary status.

For Na, the average difference (in the sense of BALDER – PHOBOS, see Figure 20) for stars with $\log_{\epsilon}(\text{Na}) > 5.25$ (indicated by the dashed line in Figure 20) was $\Delta \log_{\epsilon}(\text{Na}) = -0.19 \pm 0.06$, which includes only one AGB star. For stars with $\log_{\epsilon}(\text{Na}) < 5.25$, $\Delta \log_{\epsilon}(\text{Na}) = -0.11 \pm 0.04$ for the AGB, and $\Delta \log_{\epsilon}(\text{Na}) = -0.12 \pm 0.04$ for the RGB. This acts to reduce the 1σ spread in RGB Na abundance by 0.04 dex (to ± 0.15 dex, see Table 5), but does not alter the spread in AGB Na abundances. It also reduces the average difference in AGB and RGB Na abundance to $\Delta \log_{\epsilon}(\text{Na}) = -0.17$ from -0.22 .

For O, the average difference was $\Delta \log_{\epsilon}(\text{O}) = -0.03 \pm 0.02$ for both samples, indicating no significant difference between the O abundances determined with the two methods. We again find M 4 to be homogeneous in O. It is interesting to note that Na abundance was more sensitive than O abundance to the differences in method and atmospheric models examined in this test.

Abundances determined using the $\langle 3D \rangle$ STAGGER-grid are presented in Figure 21, along with the star-to-star differences in non-LTE Na abundance between the two sets of model atmospheres (the MARCS and $\langle 3D \rangle$ STAGGER-grid), to indicate the impact of utilising atmospheric profiles computed in $\langle 3D \rangle$ compared to 1D. The results of this test are included in Table 14, and stars that required extrapolation outside of the STAGGER-grid are indicated.

As with the MARCS grid results, use of the $\langle 3D \rangle$ STAGGER-grid for Na abundance determination gives a similar distribution to our PHOBOS v2 abundances (Figure 5). The bottom panel of Figure 21 indicates that

Table 14. Na and O abundances for each star in our M4 sample, determined using the BALDER code with i) the 1D MARCS, and ii) the ⟨3D⟩ STAGGER-grid of stellar atmospheric models (see §6.3 for details). Abundance uncertainties reflect line-to-line scatter (1σ), and do not take atmospheric sensitivities into account. The last four lines show the cluster average abundances (for the AGB and RGB) with standard error of the mean, and standard deviation to indicate observed scatter. The final column indicates, for each star, whether extrapolation in the stellar parameters was required for the analysis based on the ⟨3D⟩ STAGGER-grid. Note that the stellar parameters from Table 3 were used for all abundance determinations. Only the first five rows in the top panel are shown; the full table is available online.

ID	Type	1D MARCS		⟨3D⟩ STAGGER		⟨3D⟩ extrapolation required?
		$\log_{\epsilon}(\text{Na})$	$\log_{\epsilon}(\text{O})$	$\log_{\epsilon}(\text{Na})$	$\log_{\epsilon}(\text{O})$	
788	AGB	4.85 ± 0.03	8.20 ± 0.06	4.85 ± 0.03	8.37 ± 0.06	Yes
3590	AGB	5.06 ± 0.07	8.04 ± 0.00	5.08 ± 0.06	8.20 ± 0.01	Yes
10092	AGB	4.88 ± 0.06	8.28 ± 0.03	4.89 ± 0.05	8.42 ± 0.03	Yes
11285	AGB	5.12 ± 0.03	8.09 ± 0.04	5.13 ± 0.02	8.19 ± 0.05	Yes
13609	AGB	4.95 ± 0.06	8.10 ± 0.03	4.96 ± 0.08	8.20 ± 0.02	Yes
⋮	⋮	⋮	⋮	⋮	⋮	⋮
Mean	AGB	5.00 ± 0.03	8.15 ± 0.02	5.03 ± 0.03	8.34 ± 0.03	
σ		0.12	0.09	0.12	0.13	
Mean	RGB	5.17 ± 0.02	8.07 ± 0.01	5.21 ± 0.02	8.20 ± 0.01	
σ		0.15	0.11	0.16	0.15	

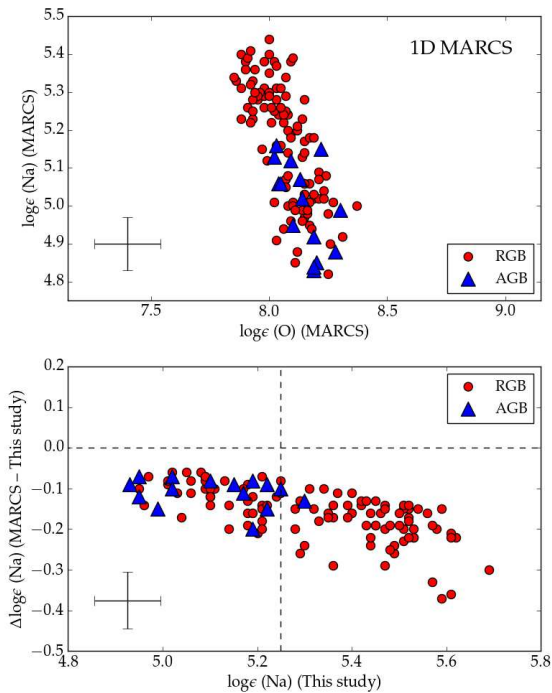


Figure 20. **Top panel:** Na and O abundances for each star in our M4 sample, determined using the BALDER code with the 1D MARCS grid of stellar atmospheric models (see §6.3 for details). Error bars indicate our total abundance uncertainties (Table 7). **Bottom panel:** The star-to-star differences in Na abundance as determined using i) the BALDER code with the 1D MARCS grid, and ii) PHOBOS v2 with the 1D ATLAS9 grid of atmospheric models. Error bars indicate our total uncertainty in Na abundance. The dashed vertical line is at $\log_{\epsilon}(\text{Na}) = 5.25$, see §6.3 for details. Note that the stellar parameters from Table 3 were used for all determinations.

the Na abundances determined with the MARCS and ⟨3D⟩ STAGGER-grid were very similar, where the average difference was $\Delta\log_{\epsilon}(\text{Na}) = -0.03 \pm 0.02$ for AGB stars, and $\Delta\log_{\epsilon}(\text{Na}) = -0.05 \pm 0.01$ for RGB stars (excluding the two brightest stars in our sample, see caption of Figure 21). The O abundances were impacted to a much higher degree; however this was mostly due to the extrapolation that was required for several stars (all AGB stars and several RGB stars required extrapolation, particularly those with high O abundances in Figure 21). The average difference in O abundance between the MARCS and STAGGER-grid was $\Delta\log_{\epsilon}(\text{O}) = -0.20 \pm 0.08$ for AGB stars, and $\Delta\log_{\epsilon}(\text{O}) = +0.13 \pm 0.08$ for all RGB stars ($\Delta\log_{\epsilon}(\text{O}) = +0.09 \pm 0.04$ excluding those that required extrapolation).

Comparing the bottom panels of Figures 20 and 21, we can see that the largest difference is between the BALDER code and PHOBOS v2, rather than between the MARCS and STAGGER-grid stellar atmospheric models. With the tests performed, however, we cannot disentangle the effects of using the ATLAS9 vs MARCS grids from the effects of using the BALDER vs PHOBOS v2 codes. For low-Na stars (including all AGB stars) there is essentially an offset when the BALDER code is used, and it compresses the range in Na by ~ 0.08 dex in high-Na RGB stars. This is independent of the choice of atmospheric model.

While the abundances of some stars are significantly different when this alternative method is employed, the overall result is unchanged, with M4 displaying an SP2 AGB deficit using both the MARCS and ⟨3D⟩ STAGGER-grids, and different abundance determination methods. It is interesting to note that the extrapolation of ⟨3D⟩ STAGGER-grid models had a large effect on O abundance, but almost no effect on Na abundance.

6.4 Full-3D STAGGER-grid results

In addition to using the ⟨3D⟩ STAGGER-grid, we also conducted a test using atmospheric models from the full-3D STAGGER-grid. This grid cannot be interpolated in T_{eff} and

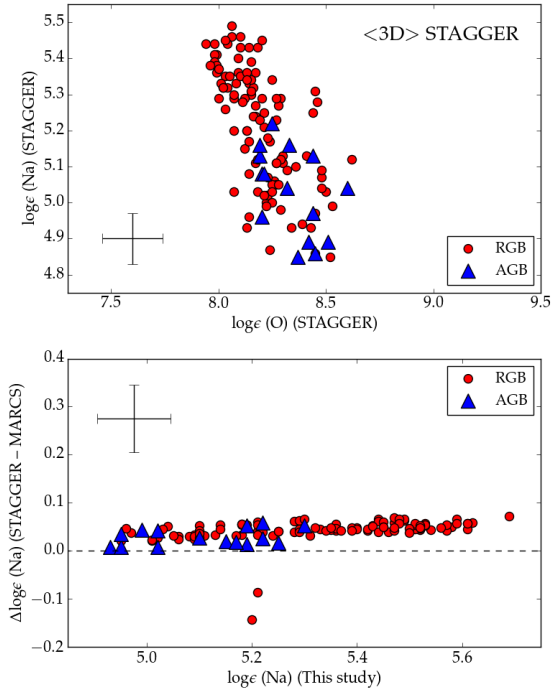


Figure 21. **Top panel:** Na and O abundances for each star in our M4 sample, determined using the non-LTE BALDER code with the (3D) STAGGER-grid of stellar atmospheric models (see §6.3 for details). Error bars indicate our total abundance uncertainties (Table 7). **Bottom panel:** The star-to-star differences in Na abundance as determined using the non-LTE BALDER code with i) the 1D MARCS, and ii) the (3D) STAGGER-grid of atmospheric models. The two outlying stars with negative differences are the two brightest stars in our sample, and were outside the STAGGER-grid by ~ 1.0 dex in $\log g$. Error bars indicate our total uncertainty in Na abundance.

$\log g$ to provide star-specific models (as with 1D grids), so only a representative test was possible. We chose three models from the STAGGER-grid, which are approximately representative of i) an upper-RGB star ($T_{\text{eff}} = 4500$ K, $\log g = 2.0$), ii) a lower-RGB star ($T_{\text{eff}} = 5000$ K, $\log g = 3.0$), and iii) an early-AGB star ($T_{\text{eff}} = 5000$ K, $\log g = 2.0$). For each model, we determined non-LTE stellar spectra in the region of the 568nm Na doublet feature at two representative Na abundances: $[\text{Na}/\text{Fe}] = 0.0$ dex ($\log_{\epsilon}(\text{Na}) \sim 5.24$), and $[\text{Na}/\text{Fe}] = 0.5$ dex ($\log_{\epsilon}(\text{Na}) \sim 5.74$).

We then computed non-LTE spectra in the same region using 1D atmospheric models using the same stellar parameters and microphysics (those used for 1D comparisons in Magic et al. 2013), and with a range of abundances between $-1.0 < [\text{Na}/\text{Fe}] < +1.2$, and microturbulence values between $1.0 < v_t < 2.0$ km/s. We quantified the corrections that should be applied to 1D Na abundances in order to account for 3D effects by comparing abundances between the 1D- and 3D-computed spectra at a given EW (corresponding to $[\text{Na}/\text{Fe}] = 0.0$ and 0.5 dex in the 3D regime).

The choice of microturbulence is vital to this test, due to the sensitivity of the corrections to v_t , which can be difficult to determine accurately (Gratton et al. 1996). We therefore interpolated the corrections based on representative v_t values for stars with T_{eff} and $\log g$ similar to the three adopted

STAGGER-grid models. All spectra were determined using the non-LTE BALDER code, as in §6.3.

Full-3D abundance corrections, as determined with the STAGGER-grid for the three representative atmospheric models, are presented in Table 15.

We found that in 3D, Na abundances are quite insensitive to changes in surface gravity – a difference of $\Delta \log g = 1.0$ only changes the Na correction by 0.02 dex, far below our total uncertainty in $\log_{\epsilon}(\text{Na})$ (± 0.07 dex). Na corrections are more sensitive to changes in effective temperature, where $\Delta T_{\text{eff}} = 500$ K alters the correction by ≤ 0.08 dex. It is important to note that significant confounding variables were unable to be accounted for in this test, including molecule (e.g. CH, NH) rearrangement due to CN processing and ‘deep mixing’ on the upper-RGB, and differences in electron number densities due to the intrinsic Na and Al abundance variations.

The primary effect of these corrections is that the 3D non-LTE distribution of RGB Na abundances would likely extend toward higher values, thus exacerbating the difference to the AGB stars. We conclude that Na-rich stars are not likely to be incorrectly identified as being Na-poor due to 3D non-LTE effects on the lines, and that using full-3D atmospheric models for our entire sample of stars would be unlikely to alter our primary result for M4.

Moreover, all of the tests here suggest that while the RGB Na dispersion can be altered with different methods and atmospheric models, the AGB stars all remain Na-poor. We found that AGB stars change in $\log_{\epsilon}(\text{Na})$ in the same direction and the same approximate magnitude as RGB stars with comparable Na abundance – we could not identify any way of systematically shifting the $\log_{\epsilon}(\text{Na})$ values of AGB stars differently to those of RGB stars. In effect, these tests retain the relative Na distributions of the AGB and RGB that we found in Section 2.4.

7 SUMMARY

In light of conflicting results in several spectroscopic studies targeting the AGB of M4, we sought to i) present robust abundances for a sample of AGB and RGB stars in M4, ii) compare these abundances to those in the recent literature to investigate whether the results agree or disagree, and iii) attempt to predict and explain the abundance distributions of AGB stars in M4.

In Section 2, we analysed a sample of 15 AGB and 106 RGB stellar spectra in M4, observed with HERMES/AAT, and originally published in ML16. We redetermined O, Na, and Fe abundances, and additionally report new Mg and Al abundances for each star. In this study, we were especially careful in our determination of stellar parameters (particularly T_{eff}), and developed our spectroscopic code PHOBOS v2 to avoid a reliance on photometric estimates of T_{eff} . We found M4 to be heterogeneous in Na and Al, while our total uncertainties in O, Fe, and Mg abundances were larger than the spread in the respective values – therefore we report that M4 is homogeneous in these species, within uncertainties. Furthermore, we found the atmospheres of our AGB sample to be lower in Na and Al, on average, compared to those of our RGB sample ($\Delta \log_{\epsilon}(\text{Na}) = -0.22$ and

Table 15. Corrections to 1D non-LTE Na abundances in order to account for 3D non-LTE effects (‘1D–3D’) for three different sets of stellar parameters, representative of i) an upper-RGB star, ii) a lower-RGB star, and iii) an early-AGB star, respectively, and for two different Na abundances. These corrections were determined using the BALDER code with the 1D MARCS grid, and full-3D STAGGER-grid of atmospheric models. Corrections were interpolated in v_t based on the typical microturbulence values of representative stars in our M4 sample.

Evolutionary Phase	Model parameters			3D–1D correction	
	T_{eff} (K)	$\log g$ (cgs)	v_t (km/s)	[Na/Fe] = 0.0 (dex)	[Na/Fe] = 0.5 (dex)
Upper-RGB	4500	2.0	1.5	0.06	0.12
Lower-RGB	5000	3.0	1.2	0.01	0.02
Early-AGB	5000	2.0	1.6	0.03	0.04

$\Delta \log_{\epsilon}(\text{Al}) = -0.14$), and with a smaller star-to-star spread in these abundances.

In Section 3, we presented new CN band strengths for a sample of 7 AGB and 19 RGB stars in M4 based on independent low-resolution spectra. We identified the bimodality in CN band-strengths that was first observed by Norris (1981), and found $\delta S3839$ to correlate with our $\log_{\epsilon}(\text{Na})$ values from §2. We found the average AGB band-strength to be weaker than that of our RGB sample ($\Delta \delta S3839 = 0.24$), and with a smaller spread in values – similar to our Na and Al results.

In Section 4, we compiled spectroscopic results from the literature. We used values from I99 (O, Na, Mg, Al, and Fe abundances), SB05 (CN band-strengths), Mar08 and Mar17 (O, Na, Mg, Al, and Fe abundances), and W17 (Na and Fe abundances). We compared the AGB and RGB distributions of $\log_{\epsilon}(X)$ and $\delta S3839$ values from these six studies to this study (as determined in §2 and §3). We found that all Fe abundance distributions agree well (both between studies, and between the giant branches within each study), except for Mar17 whose separately determined AGB and RGB abundances did not agree. We found a similar result for Mg. The uncertainties in the O abundances prevented us from drawing any conclusions for this element other than a formal homogeneity within M4 stars.

A bimodality is visible in the Na abundances of I99, Mar08/Mar17, and our work (but not W17, however this is most likely due to their large uncertainties). In the abundances of every study, the AGB samples have notably lower $\log_{\epsilon}(\text{Na})$ values, but with a bimodality still present (except W17). The Al abundances all show a similar offset between the AGB and RGB, however no bimodality could be identified, except in the results of I99 (this may be an artefact of underestimated errors and a small sample size). The CN band-strengths from SB05 and this study both show bimodality, while both AGB samples show an extreme paucity of CN-strong members.

In Section 5, we calculated a series of theoretical stellar evolutionary models with the MONSTAR code, using observational constraints on M4 stars from the literature. This was done in order to establish a precise, quantitative theoretical expectation of the abundances of AGB stars in M4. We found that in order to match the HB morphology, as determined spectroscopically by Marino et al. (2011) and Villanova et al. (2012), and using a helium enhancement for SP2 stars of $\Delta Y = 0.03$, we required a Reimers mass loss rate of $\eta = 0.44 \pm 0.03$ and initial masses of 0.827 ± 0.013 and $0.785 \pm 0.013 M_{\odot}$ for SP1 and SP2, respectively; which gave a

cluster age of 12.4 ± 0.6 Gyr. All stellar models whose HB T_{eff} matched the observed values ascended the AGB, indicating that all post-HB stars in M4, irrespective of Na abundance, should evolve to the AGB. We also demonstrated that at the metallicity of M4, only stars that reach a $T_{\text{eff}} \gtrsim 15,500$ K on the HB – 6000 K hotter than the bluest HB stars in M4 – should have AGB lifetimes short enough to avoid detection, in agreement with the models of Dorman et al. (1993).

Confronted with this discordance between our observational results and the prediction of stellar theory, we investigated the robustness of our spectroscopic abundance determinations. We did this in Section 6 by conducted a range of tests using various stellar atmospheric models in order to determine the robustness of our elemental abundance results to uncertainties in atmospheric structure. Specifically, we i) redetermined LTE Na and Fe abundances for our entire M4 sample using three different sets of photometric T_{eff} estimates (with individual T_{eff} differences of up to 500 K), ii) determined elemental abundances for a sub-sample of M4 stars using a He-enhanced ($\Delta Y = 0.10$) model from the ATLAS9 grid to estimate the effect of including He variations in atmospheric models, iii) redetermined Na and O abundances independently using the non-LTE BALDER code (Amarsi et al. 2018a) in combination with atmospheric models from the 1D MARCS grid and the (3D) STAGGER-grid, and iv) using the full-3D STAGGER-grid, determined corrections to 1D non-LTE Na abundances to account for 3D non-LTE effects for three sets of stellar parameters. All tests indicated that Na-rich stars (on the AGB or RGB) are unlikely to be misidentified as being Na-poor.

8 CONCLUSIONS

A significant strength of the spectroscopic results presented in this study (§2–3) lies in the combining of two independent methods of separating the subpopulations in chemical abundance space (using both high- and low-resolution spectra). Both of our independent sets of M4 results in this paper, namely (i) the re-analysed high-resolution spectra, with additional chemical abundances (Figure 6), and (ii) the new CN band strengths (Figure 7), support the conclusions of ML16 that AGB stars in M4 are largely representative of SP1 stars – namely, that there is a significant paucity of SP2 AGB stars, with an SP2 AGB deficit of $\mathcal{F} \gtrsim 65\%$ – as evidenced by their Na and Al abundances, and CN band-strengths, compared to those of stars on the RGB. This adds M4 to the list of GCs that have been reported to contain sig-

nificant SP2 AGB deficits, alongside NGC 6752 (Campbell et al. 2013) and M 62 (Lapenna et al. 2015).

A comparison of these results with those from the literature (§4) indicate that this is unlikely to be an artefact of our method of abundance determination: spectroscopic M 4 studies that included AGB stars have consistently shown the AGB to be systematically lower in Na abundance, Al abundance, and CN band strength (typically indicative of N abundance; Cottrell & Da Costa 1981) than the RGB – in agreement with our original findings in ML16. In stark contrast to this strong observational result, we predicted – using theoretical evolutionary models representative of M 4 stars (§5) – that the abundance distributions of the AGB and RGB should be *identical* for all species investigated in this study (except for CN due to extra mixing of N to the stellar surface on the RGB). In an attempt to reconcile the models and observations, we found that we were unable to significantly alter our abundance results by utilising a variety of atmospheric models (§6), including those with systematically offset stellar parameters, those that included a helium enhancement, different grids of 1D atmospheric models, or 3D atmospheric models.

Two recent photometric investigations of M 4 (Lardo et al. 2017, and Mar17) have reported that their data of M 4 AGB stars are consistent with the AGB containing both SP1 and SP2 stars. The spectroscopic results presented in this study similarly suggest that some proportion of SP2 stars may evolve to the AGB. However the photometric indices C_{UBI} and $C_{F275W,F336W,F438W}$ are unlikely to be precise enough to detect whether or not the most Na-enhanced SP2 stars are missing on the AGB, as suggested by the spectroscopically-determined abundances presented in this paper. We note that our CN index results – which are analogous to very narrow-band photometry – agree with the conclusions drawn from high-resolution spectroscopy, and disagree with those drawn from photometric pseudo-CMDs.

Na, Al, and N are all products of hydrogen burning (Kippenhahn & Weigert 1990), and are three of the species most commonly observed to vary among the stars of globular clusters (other species include He, C, O, and Mg; Gratton et al. 2004), both Galactic and extragalactic (Gratton et al. 2012; Brodie & Strader 2006). Of these, atmospheric Na and Al abundances are not predicted to change throughout the lives of individual present-day GC stars – these abundances are typically assumed to be an intrinsic property of the star because low-mass stars do not reach temperatures high enough to activate the Ne-Na or Mg-Al H-burning chains (Norris 1981; Iben & Renzini 1984) – while N is observed to increase on the RGB via ‘deep mixing’ (Henkel et al. 2017).

In conclusion, with no viable mechanism to reduce these abundances in-situ between the RGB and AGB, and the prediction that all stars in M 4 should evolve through to the AGB, we can see few remaining potential explanations for the consistent observations that AGB stars in M 4 have significantly lower abundances of Na, Al, and N (inferred from CN) than RGB stars in the cluster. Avenues to consider in order to resolve this disparity are diminishing, but include investigating the effect of interstellar extinction on AGB stellar spectra (M 4 experiences large differential reddening), and exploring differences between the atmospheric structures of AGB and RGB stars. We note, however, that any solution must simultaneously account for the observed

disparity in both the elemental abundance *and* CN band strength distributions, which are determined using different spectroscopic methods.

ACKNOWLEDGEMENTS

Based in part on data acquired through the AAO, via programs 09B/15, 14B/27 and 15A/21 (PI Campbell); some of these observations were conducted by Elizabeth Wylie de Boer, Richard Stancliffe, and George Angelou. Part of this work was supported by the DAAD (PPP project 57219117) with funds from the German Federal Ministry of Education and Research (BMBF). Parts of this research were conducted by the Australian Research Council Centre of Excellence for All Sky Astrophysics in 3 Dimensions (ASTRO 3D), through project number CE170100013. BTM acknowledges the financial support of the Research Training Program (RTP) scheme scholarship. SWC acknowledges federal funding from the Australian Research Council through the Future Fellowship grant entitled “Where are the Convective Boundaries in Stars?” (FT160100046). AMA acknowledges funds from the Alexander von Humboldt Foundation in the framework of the Sofja Kovalevskaja Award endowed by the Federal Ministry of Education and Research. TN acknowledges funding from the Australian Research Council (grant DP150100250). VD acknowledges support from the AAO distinguished visitor program 2016. LC gratefully acknowledges support from the Australian Research Council (grants DP150100250, FT160100402). This work was supported by computational resources provided by the Australian Government through the National Computational Infrastructure (NCI) under the National Computational Merit Allocation Scheme (project ew6). We thank Yazan Momany for providing M 4 *UBVI* photometry, and Benjamin Hendricks for providing the M 4 reddening map. We also thank Anna Marino and Yue Wang for providing additional data that aided in the literature comparison, and Yue for helpful discussions and suggestions.

REFERENCES

- AAO Software Team 2015, 2dfdr: Data reduction software, Astrophysics Source Code Library (ascl:1505.015)
- Alonso A., Arribas S., Martínez-Roger C., 1999, *A&AS*, **140**, 261
- Amarsi A. M., Asplund M., Collet R., Leenaarts J., 2016a, *MNRAS*, **455**, 3735
- Amarsi A. M., Lind K., Asplund M., Barklem P. S., Collet R., 2016b, *MNRAS*, **463**, 1518
- Amarsi A. M., Nordlander T., Barklem P. S., Asplund M., Collet R., Lind K., 2018a, preprint, ([arXiv:1804.02305](https://arxiv.org/abs/1804.02305))
- Amarsi A. M., Barklem P. S., Asplund M., Collet R., Zatsarinny O., 2018b, preprint, ([arXiv:1803.10531](https://arxiv.org/abs/1803.10531))
- Bastian N., Lamers H. J. G. L. M., de Mink S. E., Longmore S. N., Goodwin S. P., Gieles M., 2013, *MNRAS*, **436**, 2398
- Bergemann M., Nordlander T., 2014, preprint, ([arXiv:1403.3088](https://arxiv.org/abs/1403.3088))
- Brodie J. P., Strader J., 2006, *ARA&A*, **44**, 193
- Campbell S. W., Lattanzio J. C., 2008, *A&A*, **490**, 769
- Campbell S. W., Lattanzio J. C., Elliott L. M., 2006, *MmSAI*, **77**, 864

- Campbell S. W., Yong D., Wylie-de Boer E. C., Stancliffe R. J., Lattanzio J. C., Angelou G. C., Grundahl F., Sneden C., 2010, *MmSAI*, **81**, 1004
- Campbell S. W., et al., 2012, *ApJL*, **761**, L2
- Campbell S. W., et al., 2013, *Nature*, **498**, 198
- Campbell S. W., MacLean B. T., D’Orazi V., Casagrande L., de Silva G. M., Yong D., Cottrell P. L., Lattanzio J. C., 2017, *A&A*, **605**, A98
- Carretta E., et al., 2009, *A&A*, **505**, 117
- Casagrande L., Ramírez I., Meléndez J., Bessell M., Asplund M., 2010, *A&A*, **512**, A54
- Casagrande L., et al., 2014, *MNRAS*, **439**, 2060
- Cassisi S., Salaris M., Pietrinferni A., Vink J. S., Monelli M., 2014, *A&A*, **571**, A81
- Castelli F., Kurucz R. L., 2004, ArXiv Astrophysics e-prints (astro-ph/0405087),
- Catelan M., 2009, *Ap&SS*, **320**, 261
- Chantereau W., Charbonnel C., Meynet G., 2016, *A&A*, **592**, A111
- Constantino T., Campbell S., Gil-Pons P., Lattanzio J., 2014, *ApJ*, **784**, 56
- Constantino T., Campbell S. W., Lattanzio J. C., 2017, *MNRAS*, **472**, 4900
- Cottrell P. L., Da Costa G. S., 1981, *ApJL*, **245**, L79
- D’Antona F., Caloi V., Montalbán J., Ventura P., Gratton R., 2002, *A&A*, **395**, 69
- D’Antona F., Bellazzini M., Caloi V., Pecci F. F., Galleti S., Rood R. T., 2005, *ApJ*, **631**, 868
- D’Orazi V., Marino A. F., 2010, *ApJL*, **716**, L166
- Dorman B., Rood R. T., O’Connell R. W., 1993, *ApJ*, **419**, 596
- Dupree A. K., Strader J., Smith G. H., 2011, *ApJ*, **728**, 155
- García-Hernández D. A., Mészáros S., Monelli M., Cassisi S., Stetson P. B., Zamora O., Shetrone M., Lucatello S., 2015, *ApJL*, **815**, L4
- González Hernández J. I., Bonifacio P., 2009, *A&A*, **497**, 497
- Gratton R. G., Carretta E., Castelli F., 1996, *A&A*, **314**, 191
- Gratton R., Sneden C., Carretta E., 2004, *ARA&A*, **42**, 385
- Gratton R. G., Carretta E., Bragaglia A., 2012, *A&A Rev.*, **20**, 50
- Greggio L., Renzini A., 1990, *ApJ*, **364**, 35
- Grevesse N., Sauval A. J., 1998, *SSRv*, **85**, 161
- Gustafsson B., Edvardsson B., Eriksson K., Jørgensen U. G., Nordlund Å., Plez B., 2008, *A&A*, **486**, 951
- Hansen B. M. S., et al., 2002, *ApJ*, **574**, L155
- Harris W. E., 1996, *AJ*, **112**, 1487
- Hendricks B., Stetson P. B., Vandenberg D. A., Dall’Ora M., 2012, *AJ*, **144**, 25
- Henkel K., Karakas A. I., Lattanzio J. C., 2017, *MNRAS*, **469**, 4600
- Hesser J. E., Hartwick F. D. A., McClure R. D., 1977, *ApJS*, **33**, 471
- Iben I., Renzini A., 1984, *Phys. Rep.*, **105**, 329
- Ivans I. I., Sneden C., Kraft R. P., Suntzeff N. B., Smith V. V., Langer G. E., Fulbright J. P., 1999, *AJ*, **118**, 1273
- Kippenhahn R., Weigert A., 1990, Stellar Structure and Evolution Langer G. E., Kraft R. P., Friel E. D., 1985, *PASP*, **97**, 373
- Lapenna E., Mucciarelli A., Ferraro F. R., Origlia L., Lanzoni B., Massari D., Dalessandro E., 2015, *ApJ*, **813**, 97
- Lapenna E., et al., 2016, *ApJL*, **826**, L1
- Lardo C., Salaris M., Savino A., Donati P., Stetson P. B., Cassisi S., 2017, *MNRAS*, **466**, 3507
- Lattanzio J. C., 1986, *Astrophys. J.*, **311**, 708
- Leenaarts J., Carlsson M., 2009, in Lites B., Cheung M., Magara T., Mariska J., Reeves K., eds, Astronomical Society of the Pacific Conference Series Vol. 415, The Second Hinode Science Meeting: Beyond Discovery-Toward Understanding. p. 87
- Lewis I. J., et al., 2002, *MNRAS*, **333**, 279
- Lind K., Asplund M., Barklem P. S., Belyaev A. K., 2011, *A&A*, **528**, A103
- MacLean B. T., Campbell S. W., De Silva G. M., Lattanzio J., D’Orazi V., Simpson J. D., Momany Y., 2016, *MNRAS*, **460**, L69
- MacLean B. T., Campbell S. W., De Silva G. M., Lattanzio J., D’Orazi V., Cottrell P. L., Momany Y., Casagrande L., 2018, *MNRAS*, **475**, 257
- Magic Z., Collet R., Hayek W., Asplund M., 2013, *A&A*, **560**, A8
- Marigo P., Aringer B., 2009, *Astron. Astrophys.*, **508**, 1539
- Marín-Franch A., et al., 2009, *ApJ*, **694**, 1498
- Marino A. F., Villanova S., Piotto G., Milone A. P., Momany Y., Bedin L. R., Medling A. M., 2008, *A&A*, **490**, 625
- Marino A. F., Villanova S., Milone A. P., Piotto G., Lind K., Geisler D., Stetson P. B., 2011, *ApJL*, **730**, L16
- Marino A. F., et al., 2017, *ApJ*, **843**, 66
- McDonald I., Zijlstra A. A., 2015, *MNRAS*, **448**, 502
- Miglio A., et al., 2016, *MNRAS*, **461**, 760
- Milone A. P., et al., 2012, *ApJ*, **744**, 58
- Momany Y., Cassisi S., Piotto G., Bedin L. R., Ortolani S., Castelli F., Recio-Blanco A., 2003, *A&A*, **407**, 303
- Monelli M., et al., 2013, *MNRAS*, **431**, 2126
- Nardiello D., Milone A. P., Piotto G., Marino A. F., Bellini A., Cassisi S., 2015, *A&A*, **573**, A70
- Nordlander T., Lind K., 2017, *A&A*, **607**, A75
- Norris J., 1981, *ApJ*, **248**, 177
- Norris J., Cottrell P. L., Freeman K. C., Da Costa G. S., 1981, *ApJ*, **244**, 205
- Ramírez I., Meléndez J., 2005, *ApJ*, **626**, 465
- Reimers D., 1975, Memoires of the Societe Royale des Liege, **8**, 369
- Renzini A., Buzzoni A., 1986, in Chiosi C., Renzini A., eds, Astrophysics and Space Science Library Vol. 122, Spectral Evolution of Galaxies. pp 195–231, doi:10.1007/978-94-009-4598-2_19
- Saunders W., et al., 2004, in Moorwood A. F. M., Iye M., eds, Proc. SPIE Vol. 5492, Ground-based Instrumentation for Astronomy. pp 389–400, doi:10.1117/12.550871
- Sharp R., et al., 2006, in Society of Photo-Optical Instrumentation Engineers (SPIE) Conference Series. p. 62690G (arXiv:astro-ph/0606137), doi:10.1117/12.671022
- Sitnova T., et al., 2015, *ApJ*, **808**, 148
- Skrutskie M. F., et al., 2006, *AJ*, **131**, 1163
- Smith G. H., 2015, *PASP*, **127**, 1204
- Smith G. H., Briley M. M., 2005, *PASP*, **117**, 895
- Sneden C. A., 1973, PhD thesis, The University of Texas at Austin
- Sneden C., 1999, *Ap&SS*, **265**, 145
- Sneden C., Ivans I. I., Kraft R. P., 2000, Mem.Soc.Ast.It., **71**, 657
- Sousa S. G., Santos N. C., Adibekyan V., Delgado-Mena E., Israelian G., 2015, *A&A*, **577**, A67
- Spruit H. C., 2015, *A&A*, **582**, L2
- Suntzeff N. B., Smith V. V., 1991, *ApJ*, **381**, 160
- Sweigart A. V., 1997, *ApJL*, **474**, L23
- Sweigart A. V., Gross P. G., 1978, *ApJS*, **36**, 405
- Valcarce A. A. R., Catelan M., Alonso-García J., Cortés C., De Medeiros J. R., 2014, *ApJ*, **782**, 85
- Villanova S., Geisler D., Piotto G., Gratton R. G., 2012, *ApJ*, **748**, 62
- Wang Y., Primas F., Charbonnel C., Van der Swaelmen M., Bono G., Chantereau W., Zhao G., 2017, *A&A*, **607**, A135
- Yong D., et al., 2013, *MNRAS*, **434**, 3542